Blue-Green Systems

IWA PUBLISHING

Blue-Green Systems Vol 6 No 2, 264 doi: 10.2166/bgs.2024.030

Evaluation of effectiveness of Blue-Green Infrastructure for reduction of pluvial flooding under climate change and internal system failure conditions

Seith N. Mugume* and Lydia Patricia Nakyanzi

Department of Civil and Environmental Engineering, Makerere University, P.O. Box 7062, Kampala, Uganda
*Corresponding author. E-mail: smugume@gmail.com; seith.mugume@mak.ac.ug

SNM, 0000-0002-8289-0099

ABSTRACT

Blue-Green Infrastructure (BGI) has been proposed as a suitable adaptation measure that can enhance the resilience of existing urban drainage systems (UDSs). However, there are limited studies that have rigorously investigated the performance of BGI options considering future climate change and internal UDS failures. In this study, a coupled 1D–2D PCSWMM model was developed and applied to investigate the effectiveness of potential BGI options in the reduction of pluvial flooding using a case study of a 'failed' UDS in Kampala, Uganda. The study results suggest that climate change will increase the frequency of occurrence of extreme rainfall from 1 in 100 years to 1 in 10 years, thereby exacerbating the urban flooding challenge in Kampala City. The study results also ascertained that the use of spatially distributed infiltration trenches and bioretention cells at a catchment scale could lead to a modest reduction of the total flood volume and the average flood duration of at least 12.0% [9.8–14.0%] and 34.3%, respectively, when combined with improved UDS cleaning and maintenance. The findings point towards the need to implement BGI options in combination with improved asset management and investments in the expansion of grey UDSs to enhance global resilience to pluvial flooding under climate change.

Key words: Blue-Green Infrastructure, CMIP6 climate change scenarios, coupled 1D–2D modelling, internal system failures, statistical downscaling, urban flooding

HIGHLIGHTS

- Use of latest CMIP6 GCM outputs to evaluate future climate change impacts on extreme rainfall.
- Combination of coupled 1D–2D modelling and compound-threat analysis to test the effectiveness of BGI options.
- Consideration of dynamic interactions between BGI and the urban water cycle under extreme rainfall and internal system failure scenarios.
- Decentralisation and redundancy are vital in enhancing the resilience benefits of BGI.

GRAPHICAL ABSTRACT

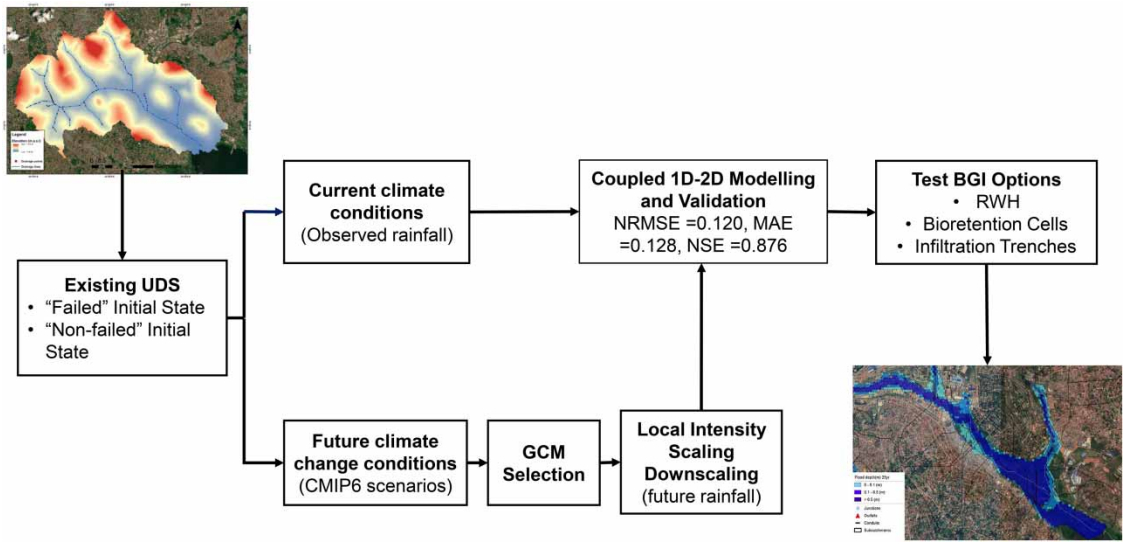

NOMENCLATURE

1D	one dimensional
1D–2D	one dimensional–two dimensional
BCC-CMC-MR	Beijing Climate Centre Climate System Model-Medium Resolution
BGI	Blue-Green Infrastructure
CMIP3	Coupled Model Intercomparison Project Phase 3
CMIP5	Coupled Model Intercomparison Project Phase 5
CMIP6	Coupled Model Intercomparison Project Phase 6
CW	catchment width
DEM	Digital Elevation Model
EPA SWMM	Environmental Protection Agency's Storm Water Management Model
GCMs	general circulation models
GFDL-ESM4	Geophysical Fluid Dynamics Laboratory Earth System Model version 4
IDF	Intensity–Duration–Frequency
IDF_CC	Intensity–Duration–Frequency Curves under Climate Change
IPCC	Intergovernmental Panel on Climate Change
IPSL-CM6A-LR	Institut Pierre-Simon Laplace Climate Model version 6A-Low Resolution
LOCI	local intensity scaling
MAE	mean absolute error
MLC	Maximum Likelihood Classification
MRI-ESM2-0	Meteorological Research Institute Earth System Model version 2.0
NetCDF4	Network Common Data Form version 4
NorESM2-MM	Norwegian Earth System Model version 2
NRMSE	Normalised Root Mean Square Error
NSE	Nash–Sutcliffe Efficiency Index
PCSWMM	Personal Computer Storm Water Management Model
PIMP	Percentage Imperviousness
RCPs	representative concentration pathways
RFSM	Rapid Flood Spreading Model
RWH	rainwater harvesting
SSPs	shared socio-economic pathway
TAMSAT	Tropical Applications of Meteorology using SATellite data and ground-based observations
UBOS	Uganda Bureau Of Statistics
UDSs	urban drainage systems

1. INTRODUCTION

Recent studies suggest that over 1.81 billion people are directly exposed to flooding (100-year return period and minimum flood depths of 0.15 m), with 89% of the aforementioned population living in low- and middle-income countries (Rentschler *et al.* 2022). In Sub-Saharan Africa, urban flooding has been exacerbated by climate change,

rapid urbanisation, insufficient coverage and capacity of existing grey urban drainage systems (UDSs), internal system failures, long-term asset deterioration, construction in low-lying flood prone areas and sea level rise (Mugume *et al.* 2017; Lumbroso 2018; The World Bank 2022; Arinabo 2023; Francisco *et al.* 2023). In Kampala city, flooding affects 170,000 people annually resulting in flooding damages estimated at US$ 49.6 million per year (World Bank 2021). Specifically, the Nakivubo urban drainage (UDS) which drains the Nakivubo catchment in Kampala's central business district is a critical drainage system that has experienced an increase in pluvial flood risk in recent years (Mugume *et al.* 2017; Arinabo 2023).

Conventional hydraulic reliability-based UDS design approaches focus on minimising the probability of occurrence of hydraulic failures resulting from a specified design storm and do not consider other causes of UDS failures (Mugume & Butler, 2017). UDS failure is defined in this research as the system's inability to safely collect, convey and dispose of storm water, wastewater or combined sewer flows leading to negative impacts such as flooding, spillage, pollution and increased risk of flood related health impacts (Mugume *et al.* 2015; Lee *et al.* 2020; Vollaers *et al.* 2021). In recent studies, UDS failures have been categorised as either functional or structural (Mugume *et al.* 2015; Dong *et al.* 2017; Mugume & Butler 2017; Yazdi 2018). Functional failures which result from hydraulic overloading are caused by extreme rainfall, urban creep, increased dry weather flows, excessive infiltration, and exfiltration. Structural failures, on the other hand, are caused by malfunction of system components such as pumps and sensors, pipe failure, gully pot and sewer blockage and deposition of sediments and solid waste in existing UDSs (Mugume *et al.* 2015, 2017; Tscheikner-Gratl *et al.* 2019; Guptha *et al.* 2022; Mcdonnell & Motta 2022; Pleau *et al.* 2022; Rosin *et al.* 2022).

Cognizant of emerging compound climate change and internal system failure threats, new resilience-based approaches that enhance flexibility, redundancy, response & recovery attributes are required to minimise flood risk in cities (Mugume *et al.* 2015, 2017). In recent research, implementation of spatially distributed Blue-Green Infrastructure (BGI) options in cities has been proposed as a suitable adaptation strategy for enhancing flexibility and redundancy attributes of existing UDSs (Kõiv-Vainik *et al.* 2022; Sitzenfrei *et al.* 2022; Ortega Sandoval *et al.* 2023; Mugume *et al.* 2024; Osheen *et al.* 2024). BGI includes both natural and engineered systems that can enhance the physical, chemical and microbiological quality of stormwater in cities (Neumann *et al.* 2024).

However, there is still a low uptake of BGI options at the city scale due to various socio-economic, institutional and political barriers and the lack of standardised guidelines for the design and optimal location of new BGI in cities (Drosou *et al.* 2019; Alves *et al.* 2020; Kuller *et al.* 2021; Pauleit *et al.* 2021). A number of recent studies have investigated the effectiveness of implementing BGI options that include rainwater harvesting (RWH) systems, infiltration trenches, bioretention cells, detention ponds, green roofs and permeable pavements in the reduction of urban flooding (Webber *et al.* 2020; Rodriguez *et al.* 2023; Mugume *et al.* 2024; Neumann *et al.* 2024). Most of these BGI modelling studies suggested that BGI options designed using current design standards are most cost-effective during moderate rainfall with return periods of up to 10 years (Mugume *et al.* 2024). In addition, these studies have highlighted that residual flood risk remains particularly caused by the occurrence of extreme rainfall events (Webber *et al.* 2020), failure of existing UDSs that receive flows from BGI (Mugume *et al.* 2024) and malfunction of individual BGI units (Funke & Kleidorfer 2024).

In addition, there are limited studies that have rigorously investigated the performance of BGI options considering a combination of future climate change (Jiang & McBean 2021; Guptha *et al.* 2022; Pons *et al.* 2022; Yang *et al.* 2022) and internal UDS failures (Mugume *et al.* 2024). In recent studies, the Coupled Model Intercomparison Project Phase 5 (CMIP5) general circulation model (GCM) results have been applied to investigate the performance of BGI under future climate change. CMIP5 GCM results are generated based on two representative concentration pathways (RCPs) representing medium (RCP4.5) and high (RCP8.5) future emissions scenarios based on projected radiative forcing components (Leandro *et al.* 2020; Jiang & McBean 2021; Nadoya *et al.* 2022). However, despite the notable improvement of CMIP5 extreme rainfall projections when compared to earlier Coupled Model Intercomparison Project Phase 3 (CMIP3) model outputs, large spatial and temporal uncertainties still exist in tropical East Africa (Zebaze *et al.* 2019; Akinsanola *et al.* 2021), suggesting the need to utilise more recent and accurate CMIP6 GCM results (IPCC 2021).

In recent work, Jiang & McBean (2021) modelled combinations of BGI options (RWH, swales, bioretention cells, and permeable pavements) using the PCSWMM model at a lot-scale to investigate their effect on the reduction of runoff volume and peak flows in London, Ontario, Canada. The impacts of climate change on extreme rainfall intensities were assessed using the web-based IDF_CC tool using CIMP5 GCM results for the

RCP8.5 scenario (Schardong *et al.* 2020). The study results suggested that the considered BGI options could provide effective control for water quantity for rainfall events with low return periods of 2–5 years.

Furthermore, Pons *et al.* (2022) applied a multiplicative random cascade approach to generate future rainfall time series, considering the RCP 8.5 scenario. The future rainfall time series was applied to investigate the performance of green roofs in eight locations in Norway and France. The study results suggested that the performance of green roofs decreased in most Norwegian cities (due to an increase in precipitation), but improved in Marseille, France (due to a decrease in rainfall event frequency). Yang *et al.* (2022) investigated the hydraulic and water quality performance of BGI in Chaohu City, China, using downscaled CMIP5 GCM projections. The study results demonstrated that the BGI options in the given areas mitigated runoff volume, peak flow, and non-point pollution by 45–80%, 39–60%, and 31–82%, respectively, but declined under all considered RCP future climate scenarios.

However, these studies were undertaken using CIMP5 GCM results which exhibit large spatial and temporal uncertainties in the projection of extreme rainfall over East Africa (Zebaze *et al.* 2019; Akinsanola *et al.* 2021). In a recent study, Yao *et al.* (2023) utilised CMIP6 simulated rainfall data, for the shared socio-economic pathway (SSP) scenarios (SSP1-2.6, SSP2-4.5 and SSP5-8.5) to investigate the effect of a combination of BGI (rain gardens, green roofs, permeable pavements) and grey infrastructure options (strong tanks and rehabilitation of UDS using large diameter pipes) on enhancement of resilience of an existing UDS in Xiao Zhai area in Xi'an City, China. The study results suggested that the considered Grey-Green Infrastructure (GGI) increased the resilience index from a range of 0.36–0.89 to 0.67–0.95 representing an 85% increase. Furthermore, Wang *et al.* (2023) utilised the recent CMIP6 GCM results to undertake continuous simulation of the performance of spatially optimised GGI options using a case study of Guangzhou city in Southern China. The study results suggested that increased spatial distribution of the proposed GGI solutions significantly improved global UDS resilience to flooding under future climate change. In addition, Zhang *et al.* (2024) applied a multi-objective optimisation approach to adjust the spatial layout of Green Infrastructure in Lanzhou City, Chengguan, Northwest China. However, the application of CMIP6 GCM results to investigate the performance of BGI in cities is still limited (Wang *et al.* 2023; Yao *et al.* 2023; Zhang *et al.* 2024).

To the author's knowledge, there are no studies that have investigated the effectiveness of BGI when subject to compound climate change and internal system failure threats. Furthermore, there are limited studies that have utilised the latest CMIP6 GCM model outputs to investigate BGI performance (Wang *et al.* 2023; Yao *et al.* 2023). The latest CMIP6 global climate model experiments considered an ensemble of over 23 GCMs and a more comprehensive experimental design which enabled a more accurate representation of physical, chemical and biological processes at higher spatial and temporal resolution (Meinshausen *et al.* 2020; IPCC 2021; Nadoya *et al.* 2022; Siabi *et al.* 2023). In addition, the CMIP6 GCM results utilised the recent SSPs and radiative forcing scenarios leading to more accurate future climate change simulation results at regional scales (Eyring *et al.* 2016; O'Neill *et al.* 2016; Riahi *et al.* 2017; Meinshausen *et al.* 2020; Dong & Dong 2021; Rhymee *et al.* 2022; Wang *et al.* 2023).

In this study, a coupled 1D–2D model of the existing Nakivubo urban drainage system (UDS) in Kampala City was developed and utilised to investigate the performance of an existing UDS considering dual threats, that is: future climate change and internal UDS failures. The impacts of future climate change on urban rainfall in Kampala were quantified using statistically downscaled SSP2-4.5 and SSP5-8.5 scenarios from the latest CMIP6 global climate model outputs for the near future period (2050). The resulting flooding impacts were quantified by considering 'failed', 'partially-failed' and 'non-failed' UDS initial states, using total flood volume and average flood duration as system performance indicators (Mugume *et al.* 2024). Furthermore, the developed coupled 1D–2D model was applied to test the effectiveness of potential BGI options with respect to the reduction of flooding impacts.

Using the developed methodology, the overarching objective of the research that entailed investigation of the effect of compound future climate change and internal system failure threats on the performance of spatially distributed BGI options with respect to the reduction of urban pluvial flooding was investigated. Furthermore, the main research questions that formed the basis of the research are presented:

(a) What is the effect of future climate change, assessed using the latest CMIP6 GCM outputs on pluvial flooding in Kampala City?
(b) How do compound climate change and internal UDS failure threats affect the performance of existing UDSs?

(c) How effective are RWH systems, infiltration trenches and bioretention cells in reducing urban flooding in existing grey UDSs under future climate change and internal system failure conditions?

The novelty of this research lies in application of a combination of a more complex coupled 1D–2D urban flood modelling approach and rigorous compound-threat analysis (consideration of future climate change using the latest CMIP6 GCM results and internal system failures) to investigate the effectiveness of BGI in enhancing the resilience of an existing UDS in the highly urbanised catchment. The adopted approach has enabled consideration of dynamic interactions between BGI elements, the urban water cycle under extreme climate and internal system failure conditions and provides a more realistic view of the effectiveness of BGI for the reduction of pluvial flood risk in cities.

2. METHODOLOGY

In this research, a methodology that combines coupled 1D–2D urban drainage modelling and failure modelling was applied to investigate the performance of BGI for the reduction of urban flooding in Kampala, Uganda. Functional failures were assessed by simulating UDS performance considering different rainfall intensities and return periods, T for both current and projected future climate change. Assessment of the impacts of future climate change was undertaken using the latest SSP scenarios that include: SSP2-4.5 and SSP5-8.5 for five selected general circulation models (GCMs). Internal UDS failures, on the other hand, were considered in the UDS using 'failed', 'partially-failed' and 'non-failed' initial states (Mugume *et al.* 2015). The proposed study approach which was adapted from Mugume *et al.* (2024) is illustrated in Figure 1.

2.1. Projection of future climate change impacts on urban rainfall

In recent studies, it has been argued that the use of the recent CMIP6 data results in more accurate future climate change projections over Uganda when compared to the CMIP5 data. This is attributed to the use of more comprehensive and robust GCMs with more sophisticated physics and higher resolution for the simulation of CMIP6 global climate model outputs (Nadoya *et al.* 2022). In addition, the use of recent SSPs (Meinshausen *et al.* 2020) provides a more accurate description of socio-economic developments that influence the emission of green house emissions as opposed to RCPs that only consider projections of radiative forcing components (van Vuuren *et al.* 2011)

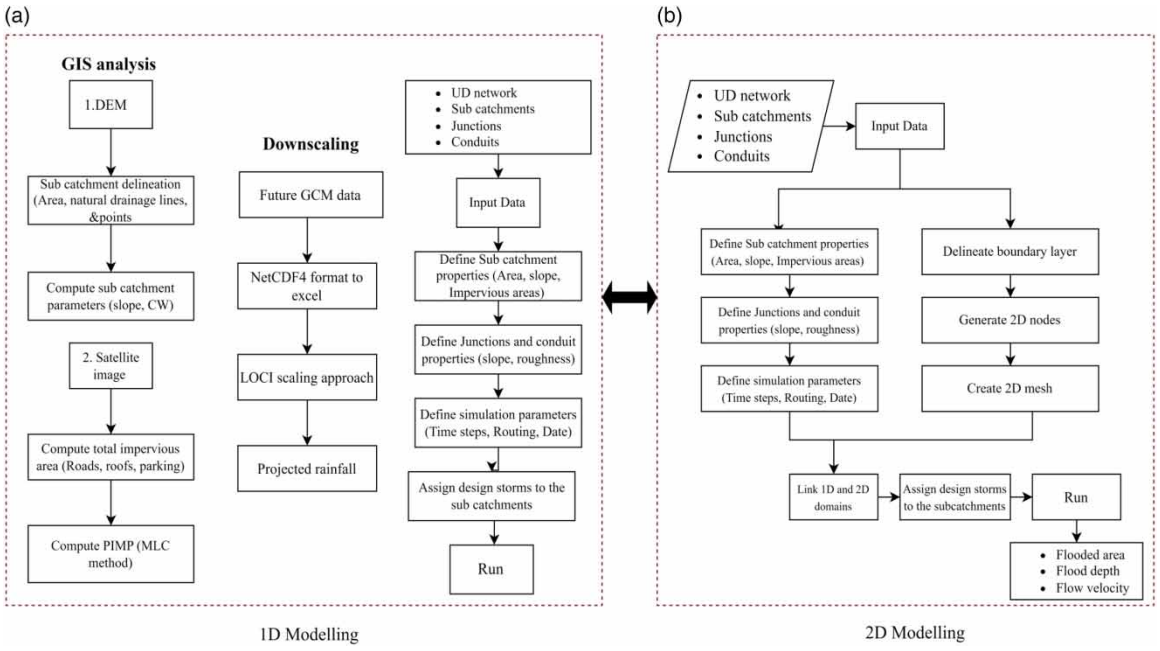

Figure 1 | Adopted study approach.

2.1.1. CMIP6 global climate model results

In this research, historical and future CMIP6 climate datasets downloaded from the Copernicus climate data base (Buontempo *et al.* 2022) were utilised for evaluation of the impact of climate change on rainfall in Kampala city. Two time scales, that is a historical baseline (1991–2020) and a near future projected 2020–2049 (2050) period, were considered in this study. Furthermore, two SSP future scenarios, SSP 2-4.5 and SSP 5-8.5, representing medium and high emission scenarios, respectively, were projected using a multi-model ensemble of five GCMs: NorESM2-MM, MRI-ESM2-0, GFDL-ESM4, BCC-CMC-MR and IPSL-CM6A-LR (Table 1). The selection of these GCMs was based on their demonstrated ability to accurately replicate rainfall patterns in Uganda (Nadoya *et al.* 2022) and their accessibility within the Kampala Grid, covering the geographical coordinates of 0.3184°N and 32.36°E, including the Makerere University meteorological centre, the source of observed meteorological data.

The SSP 2-4.5 is a medium forcing (4.5 W/m^2 radiative forcing) and the most plausible scenario that aligns with climate actions aimed at meeting existing emission reduction obligations, while SSP 5-8.5 (8.5 W/m^2 radiative forcing) represents an extreme scenario envisioning global economic growth driven by natural gas, oil, and coal combustion, exacerbating climate change (Nadoya *et al.* 2022; Siabi *et al.* 2023). Historical and projected rainfall data for the five GCMs under SSP 2-4.5 and SSP 5-8.5 scenarios for the period 1991–2049 were downloaded in the NetCDF4 format and categorised into the baseline period (1991–2020) and the near future (2020–2049). Statistical downscaling using regression techniques was undertaken to match the local climate at the catchment scale (Rhymee *et al.* 2022).

2.1.2. Local intensity scaling statistical downscaling approach

The local intensity scaling (LOCI) method was applied to correct the frequency and intensity of wet days through the elimination of drizzle days (days with little rainfall) in the GCM raw data (Schmidli *et al.* 2006; Nakkazi *et al.* 2022). This approach entails two steps. In the first step, a wet-day threshold for the m^{th} month $P_{thres,m}$ is determined from the raw GCM rainfall time series to ensure that the threshold exceedance matches the wet-day frequency of the observed rainfall. In the second step, a scaling factor, s_m (Equation (1)) is calculated and used to ensure that the mean of the corrected rainfall is equal to that of the observed rainfall (Equation (2)) (Teutschbein & Seibert 2012; Fang *et al.* 2015; Shrestha 2016).

$$s_m = \frac{\mu(P_{obs,m,d}|P_{obs,m,d} > 0}{\mu(P_{raw,m,d}|P_{raw,m,d} > P_{thres,m}} \tag{1}$$

$$P_{cor,m,d} = \left\{ \begin{matrix} 0, & if\ P_{raw,m,d} < P_{thres,m} \\ P_{raw,m,d} \cdot s_m, & otherwise \end{matrix} \right\} \tag{2}$$

where $P_{obs,m,d}$ is the observed daily rainfall; $P_{raw,m,d}$ is the simulated raw daily GCM rainfall and $P_{cor,m,d}$ is the bias-corrected daily rainfall.

The projected future rainfall for the considered GCMs was analysed and bias corrected using the described LOCI method. Using the bias-corrected projected future rainfall, new Intensity–Duration–Frequency (IDF) curves were developed using the Watkins and Fiddes procedure (Watkins & Fiddes 1984). Furthermore, 10-

Table 1 | Selected CIMP6 global climate models employed in the study

Global climate model (GCM)	Institution	Spatial resolution (Lat × Lon)	Temporal resolution	Source
GFDL-ESM4	Geophysical Fluid Dynamics Laboratory (GFDL), USA	2.81° × 2.81°	daily	Dunne *et al.* (2020)
BCC-CSM2-MR	Beijing Climate Center, China	1.0° × 1.0°	daily	Wu *et al.* (2021)
IPSL-CM6A-LR	Institut Pierre-Simon Laplace, France	1.25° × 2.5°	daily	Dong & Dong (2021)
NorESM2-MM	Norwegian Climate Centre, Norway	1.875° × 2.5°	daily	Seland *et al.* (2020)
MRI-ESM2-0	Meteorological Research Institute (MRI), Japan	1.125° × 1.125°	daily	Kawai *et al.* (2019)

year return period design storms were obtained using the alternate block method (Balbastre-Soldevila *et al.* 2019). Change factors for all GCMs under various scenarios were determined relative to present climate conditions using design storms, illustrating the effects of climate change on future rainfall.

2.2. Modelling of surface flooding

The main approaches for modelling surface flooding can be broadly categorised as one dimensional (1D), dual drainage or 1D-1D, 2D surface flood spreading models and coupled 1D–2D modelling (Mugume 2015; Butler *et al.* 2018). In 1D modelling, surface flooding from the minor system is temporarily stored as exceedance flows at the top of nodes using 'virtual flood cones'. In the 1D modelling approach, the overland flows that occur in the major drainage system are excluded from the analysis (Mugume 2015; Rossman 2016; Butler *et al.* 2018). In contrast to the 1D modelling approach, the 1D-1D modelling approach enables distinct consideration of vertical interactions between the major and minor system flows (Djordjević *et al.* 1999; Schmitt *et al.* 2005; Maksimović *et al.* 2009) and enables more accurate description of the transitions from free surface flows in the *minor system* to surcharging (pressurised flow), and finally to occurrence of overland flows in the *major system* that are modelled as a network of ponds and pathways (Djordjević *et al.* 2005; Ryu 2008; Maksimović *et al.* 2009; Mugume 2015; Butler *et al.* 2018). The 2D Rapid Flood Spreading Models (RFSMs) on the other hand build on and extend the 1D approach through a realistic distribution of the total flood volume generated by the minor system model over the catchment surface (Ryu 2008; Blanc *et al.* 2012; Butler *et al.* 2018).

In this research, coupled 1D–2D modelling, which provides a more accurate approach for the simulation of surface flooding when compared to 1D, 1D-1D and 2D RFSMs was applied (refer to Supplementary Information, Section 2 for a detailed comparison of urban drainage modelling approaches). This approach utilises a network of 2D grid cells and can represent bidirectional flow between the 1D and the 2D domains using direct links or weir/orifice type elements and enables a more realistic representation of system flows during extreme events in which surface flows are not confined to streets or road profiles (Maksimović *et al.* 2009; Digman *et al.* 2014; Leandro & Martins 2016; Ortega Sandoval *et al.* 2023; Mugume *et al.* 2024). It also enables a more exact representation of buildings and urban structures which facilitates a more realistic analysis of surface flows during flooding conditions (Maksimović *et al.* 2009).

Furthermore, coupled 1D–2D modelling was undertaken in PCSWMM v7.5.3406, a physically based coupled 1D–2D model developed by Computation Hydraulics International Ontario, Canada (Chitwatkulsiri *et al.* 2022; Manchikatla & Umamahesh 2022; Ortega Sandoval *et al.* 2023). PCSWMM utilises the US EPA SWMM 5.0.015 hydrology and hydraulics engine that is primarily developed for modelling of water quantity and quality in urban areas for both short- and long-term simulation runs (Rossman 2016). The key components and features that require representation in the model include urban hydrological modelling, 1D-hydraulic modelling, and the coupled 1D–2D modelling.

The main steps entailed in the adopted coupled 1D–2D modelling approach include the delineation of a bounding layer, 2D node generation, 2D mesh creation, and the connection of each junction in the 1D model to the closest 2D junctions. The adopted coupled 1D–2D modelling approach is graphically illustrated in Figure 1. (Ortega Sandoval *et al.* 2023; Mugume *et al.* 2024).

2.3. Modelling of internal UDS failures

Three UDS initial system states that are 'failed', 'partially-failed', and 'non-failed,' were considered in the study. The 'failed' UDS initial state represents the 'worst-case' UDS initial state condition in which all links (conduits) have experienced complete structural failure caused by pipe failures, collapsed open channel sections, blockages, deposited sediments and solid waste, which collectively limit the hydraulic conveyance capacity of the existing UDS. In this initial state, a Manning's n value of 100 is assigned to all links, reflecting the asset condition typical in many developing country cities with inadequate cleaning and maintenance and the presence of deposited sediments and solid waste (Mugume *et al.* 2015, 2024).

On the other hand, the partially 'failed' UDS initial state represents the current condition in which links in the UDS have experienced partial failures or are partially filled with deposited sediment and solid waste resulting in the reduction of the hydraulic conveyance capacity of the UDS. In this initial state, a Manning's n value of 0.063, which represents a 50% reduction in the peak flows, was applied for coupled 1D–2D modelling to determine the 2D surface flooding extents corresponding to 50% failure (refer to Supplementary Information, Section Table S6).

On the other hand, the 'non-failed' UDS initial state represents the ideal condition where all links are well-maintained, clean, structurally sound, free of sediments or solid waste, and meet the designed hydraulic conveyance capacity. A Manning's n value of 0.020 is used to model all links in the 'non-failed' system (Mugume *et al.* 2015). Employing the adopted failure modelling approach can enable a quantitative assessment of the effectiveness of UDS cleaning, repair, and maintenance strategies, which can complement the benefits of BGI (Mugume *et al.* 2024).

2.4. Case study 1D–2D model set up

2.4.1. Datasets used in the study

The datasets utilised include a 5 m horizontal resolution Digital Elevation Model (DEM), soil and land use maps, existing UDS hydraulic parameters (bottom width, top width, side slopes & invert levels), and observed hydrometeorological data (Table 2). GIS-based spatial analysis of the DEM was applied to delineate the catchment into 47 sub-catchments. Zonal analysis was carried out to obtain the average slopes of each delineated sub-catchment, which ranged from 0.045 to 0.156. The iterative supervised classification which is a form of the maximum likelihood classification approach (Han & Burian 2009) was used to compute the Percentage Imperviousness (PIMP) for the Nakivubo catchment as 64.4%. Furthermore, a 77-year observed daily rainfall dataset for Makerere University meteorological station was used in this study. The main steps entailed in the extreme rainfall analysis include: extraction of maximum daily rainfall for each month and year, derivation of IDF curves using the Annual Maximum Series method, determination of the 2-year–24 hr rainfall and derivation of design rainstorms using the alternating block method (Fiddes *et al.* 1974; Mugume & Butler 2017; Butler *et al.* 2018; Mugume *et al.* 2024).

2.4.2. Description of the existing Nakivubo UDS

A real-world case study UDS that drains the Nakivubo catchment in Kampala city was used in this research. The location of the Nakivubo catchment and the major drainage catchments of Kampala including Kinawataka (32.7 km^2), Lubigi (64 km^2) and Nalukolongo (33.1 km^2) are shown in Figure 2.

The Nakivubo catchment drains a total area of 39.1 km^2, delinated into 47 sub-catchments. The catchment is highly urbanised with mixed developments that include high income industrial and commercial areas in Lugogo industrial areas, the Central business district as well as low to medium income areas located upstream of the catchment which includes parts of Makerere University.

The existing primary and secondary drainage systems comprise a network of pipes, trapezoidal open sections, and bridge and culvert crossings (Mugume *et al.* 2015). The modelled Nakivubo UDS is 12.3 km long and comprises a dendritic network of 177 conduits and 177 nodes. The average sub-catchment slope and PIMP were

Table 2 | Datasets used in the study

Data classification	Dataset	Data Quality	Period/ Publication year	Data source/ Website
Topographic	DEM	5 × 5 m spatial resolution	2016	Kampala Capital City Authority (KCCA)
Soil	Soil map	250 × 250 m spatial resolution	2015	Food and Agricultural Organization (FAO), https://www.fao.org/soils-portal/data-hub/soil-maps-and-databases/faounesco-soil-map-of-the-world/en/
Land use	Land cover maps	30 × 30 m	2018	United States Geological Survey (USGS), https://earthexplorer.usgs.gov/
Hydraulic	UDS properties		2016	Kampala Drainage Master Plan
Climatological – Observed	Precipitation	Daily 4 × 4 km	1991–2019 1991–2019	Makerere University Meteorological Centre Tropical Applications of Meteorology using SATellite data and ground-based observations (TAMSAT), https://data.tamsat.org.uk/data-download/rainfall/
Climatological – Projected	Precipitation	Daily temporal resolution	2020–2049	Copernicus, https://climate.copernicus.eu/

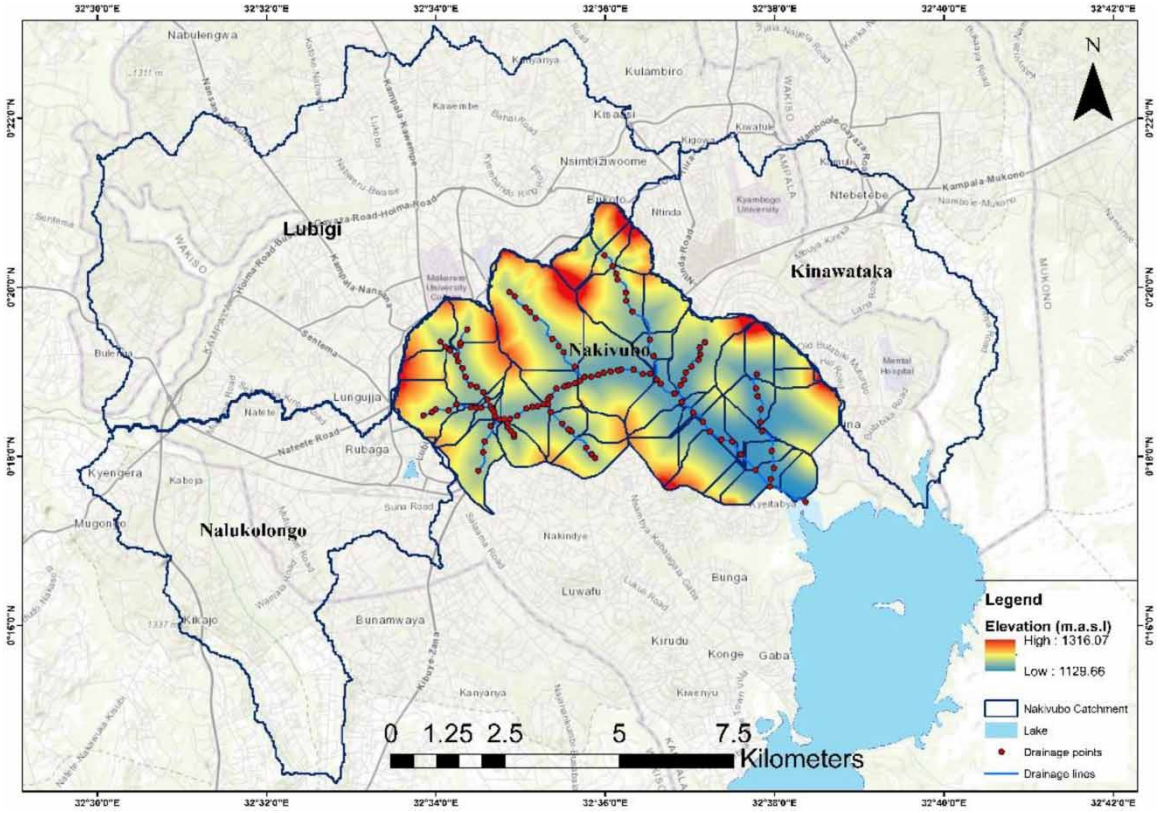

Figure 2 | Location of the Nakivubo catchment in Kampala.

computed as 7.7% [0.5–15.7%] and 64.4%, respectively. Using the analysed input data, detailed hydrological and hydraulic models of the Nakivubo UDS were built in PCSWMM v7.5.3406. A detailed description of the 1D hydrological and hydraulic modelling is provided by Mugume *et al.* (2024).

Furthermore, a set of design rainstorms with a fixed duration of 24 h and return periods, *T* of 2, 5, 10, 25 50 and 100 years were used in the model (hereafter referred to as *T2*, *T5*, *T10*, *T25*, *T50* and *T100*, respectively) for the current climate analysis. For the projected future climate change analysis, downscaled rainfall events with a return period of 10 years for each selected GCM and considering both SSP2-4.5 and SSP5-8.5 scenarios were used to run the model. Furthermore, the rainstorms were applied uniformly across all the sub-catchments within the catchment.

2.5. Modelling of BGI options

RWH tanks, infiltration trenches, and bioretention cells were modelled in PCSWMM, considering spatial coverages that ranged from 0.3 to 1.1% of the total catchment area. The BGI options were modelled to treat runoff from 60 to 20% of the of the impervious pervious areas, respectively. Each BGI option was modelled independently while maintaining the same overall storage volume. Based on an estimate of the number of homes within the catchment, RWH's spatial coverage was determined. Official national population data was used to analyse the population within the catchment (UBOS 2020). Using the assessed population data and assuming an average household size of four persons in Kampala (Mugume *et al.* 2017) and considering that 70% of the households install a RWH tank, the total volume allocated to RWH was determined as 239,753 m^3 for Nakivubo catchment (refer to Supplementary Information, Table S7).

To enable comparative evaluation of the effectiveness of singular BGI options in the reduction of pluvial flooding, the same retained volume (239,753 m^3) was specified for each BGI option. The total number of units of each BGI option is presented in Supplementary Information, Table S8. A total of 47,951 RWH units with a total storage volume of 239,753 m^3 were modelled in PCSWMM as 'rain barrels' and were spatially distributed in all the sub-catchments. The RWH units are assumed to be empty prior to the start of the rainfall event. Furthermore, a drain delay of 6 h was adopted for modelling purposes. In addition, a total of 2,664 spatially distributed

infiltration trenches are modelled in PCSWWM, each with an area of 150 m^2 and a volume of 90 m^3. The hydraulic conductivity and porosity values of 70.8 mm/hr and 0.30 were applied in the model (Havik 2012). Finally, a total of 3,330 spatially distributed bioretention cells were modelled in PCSWWM at a sub-catchment level. The hydraulic void ratio and seepage rates of 0.4 and 70.8 mm/year were applied in the model (Havik 2012).

2.6. Model validation

Field surveys provide a useful tool that enables an improved understanding of the physical behaviour of extreme events such as floods, tsunamis, or hurricanes (Wüthrich *et al.* 2024). In this research, model validation was undertaken by comparing field measurements of the observed maximum flood depths at 20 selected flood hotspot locations in the catchment, with corresponding values of the simulated flood depths (Figure 3).

For each of the selected locations, the coordinates and simulated flood depth were extracted from the PCSWMM model and compiled in a field flood depth validation sheet. Thereafter, field visits to each of the 20 selected flood hotspot locations were undertaken. During the field visits, the observed maximum flood depth at each location was measured as a vertical distance between the ground level and the highest flood mark on existing buildings (Wüthrich *et al.* 2024). In some instances, the validation process also involved interviewing residents to confirm the maximum flood levels at some of the buildings.

Furthermore, the coordinates of each location were obtained using a mobile GPS application (Mugume *et al.* 2024). Georeferencing was applied to confirm the coordinates of selected locations with corresponding coordinates extracted from the PCSWMM. Any discrepancies in coordinates were documented, and the field coordinates were crosschecked to ensure a more accurate comparison of the field and simulated flood depths. The corresponding simulated flood depth at each selected location was extracted from the flood depth map and the results were compared (Mugume *et al.* 2024). This methodology aligns with recent studies, where post-event surveys of reported flooding impacts were used to validate flood modelling results (Varlas *et al.* 2019; Mugume *et al.* 2024; Wüthrich *et al.* 2024).

The Nash–Sutcliffe Efficiency (NSE) Index, the mean absolute error (MAE) and the normalised root mean square error (NRMSE) were used as performance indicators to evaluate the goodness of fit between the observed

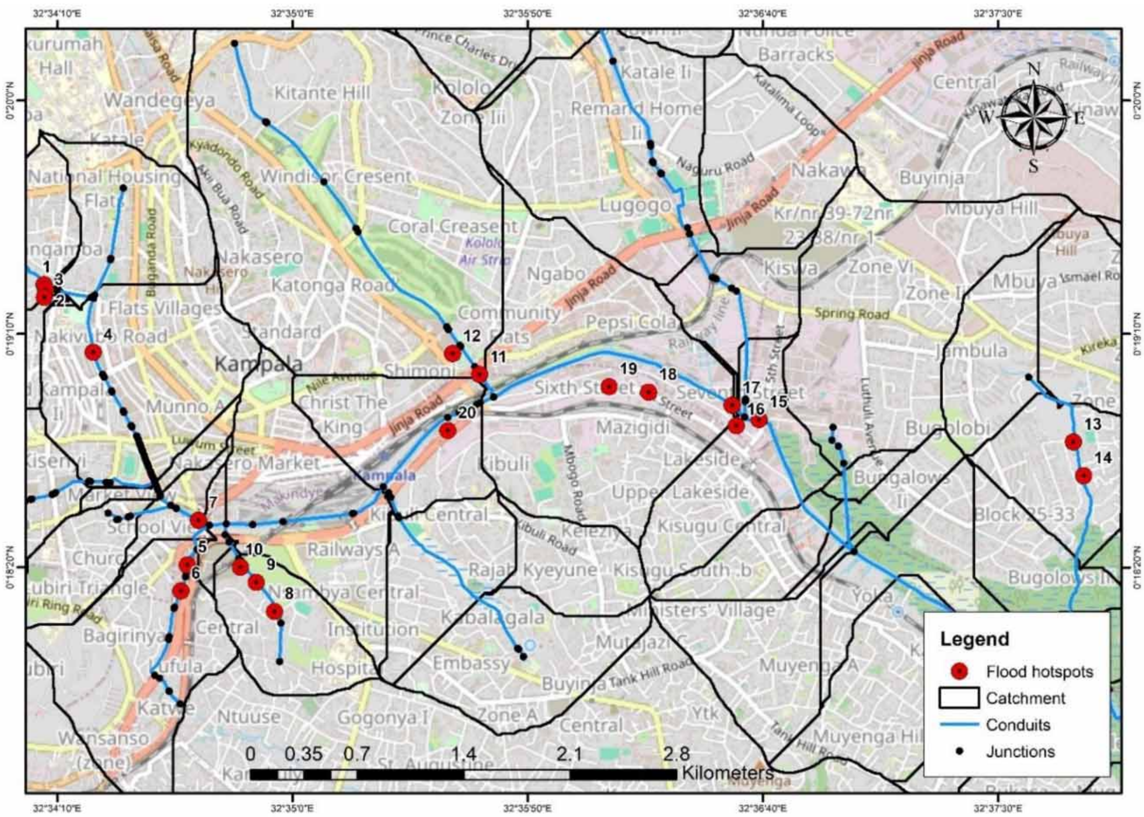

Figure 3 | Location of selected flooding hotspots.

maximum and simulated flood depths (Equations (3), (4) and (5)). The NSE Index values range from negative infinity to 1 (Equation (3)). Values between 0 and 1 are generally acceptable, with NSE = 0.65 considered as unsatisfactory; NSE = 0.80 as acceptable; NSE = 0.90 as good; and NSE > 0.90 as very good (Ritter & Muñoz-Carpena 2013).

$$NSE = 1 - \frac{\sum_{t=1}^{t_y} (d_o^t - d_m^t)^2}{\sum_{t=1}^{t_y} (d_o^t - \overline{d_o})^2} \tag{3}$$

$$NRMSE = \frac{\sum (d_m - d_0)^2}{\sum d_o^2} \tag{4}$$

$$MAE = \frac{1}{N} \sum_{I=1}^{N} |d_m - d_o|^2 \tag{5}$$

where $\overline{d_o}$ is the mean of the observed flood depths; d_m is the simulated flood depth; d_o^t is the observed flood depth at time t and N is the number of observations.

3. RESULTS AND DISCUSSION

3.1. Model validation

The computed NSE values for the catchment were 0.841 and 0.876, considering the *T25* and *T50* rainfall return periods, respectively. This suggests that the measured maximum flood depths were attributed to pluvial flooding events with return periods ranging from 25 to 50 years (Table 3). Furthermore, the computed NRMSE values were

Table 3 | Coupled 1D–2D flood model validation results

Location ID	Coordinates		Simulated flood depth (m)						RMSE parameter (dm -ds)^2				
	Long.	Lat.	Measured flood depth (m)	T5	T10	T25	T50	T100	T5	T10	T25	T50	T100
NA-1	32.5687	0.3224	0.20	0.14	0.18	0.20	0.24	0.38	0.00	0.00	0.00	0.00	0.00
NA-2	32.5688	0.3221	0.28	0.17	0.21	0.24	0.32	0.42	0.01	0.00	0.00	0.00	0.00
NA-3	32.5687	0.3216	0.19	0.11	0.13	0.16	0.25	0.29	0.01	0.00	0.00	0.00	0.00
NA-4	32.5716	0.3184	0.72	0.34	0.47	0.58	0.61	0.74	0.15	0.06	0.02	0.01	0.01
NA-5	32.5772	0.3057	0.12	0.00	0.01	0.02	0.03	0.16	0.01	0.01	0.01	0.01	0.00
NA-6	32.5778	0.3084	0.22	0.02	0.03	0.03	0.09	0.17	0.04	0.04	0.04	0.02	0.26
NA-7	32.5823	0.3029	0.68	0.29	0.31	0.45	0.53	0.56	0.16	0.14	0.06	0.02	0.06
NA-8	32.5812	0.3047	0.35	0.15	0.19	0.24	0.25	0.28	0.04	0.03	0.01	0.01	0.10
NA-9	32.5803	0.3056	0.33	0.17	0.21	0.24	0.29	0.84	0.03	0.01	0.01	0.00	0.00
NA-10	32.5944	0.3170	0.60	0.14	0.22	0.55	0.58	0.85	0.21	0.14	0.00	0.00	0.34
NA-11	32.5928	0.3183	0.82	0.38	0.55	0.70	0.73	1.14	0.20	0.08	0.02	0.01	0.02
NA-12	32.5768	0.3042	0.95	0.41	0.60	0.74	0.78	0.94	0.29	0.12	0.04	0.03	0.01
NA-13	32.6295	0.3130	1.06	0.16	0.23	0.29	0.32	0.48	0.81	0.69	0.59	0.55	0.09
NA-14	32.6301	0.3110	0.52	0.03	0.11	0.16	0.19	0.39	0.24	0.17	0.13	0.11	0.01
NA-15	32.6109	0.3144	0.75	0.32	0.45	0.61	0.65	0.84	0.19	0.09	0.02	0.01	0.00
NA-16	32.6096	0.3140	0.78	0.49	0.62	0.77	0.80	1.08	0.08	0.03	0.00	0.00	0.00
NA-17	32.6093	0.3152	0.67	0.38	0.49	0.64	0.68	0.78	0.09	0.03	0.00	0.00	0.04
NA-18	32.6044	0.3160	0.39	0.03	0.16	0.32	0.38	0.44	0.13	0.05	0.00	0.00	0.00
NA-19	32.6020	0.3163	0.42	0.01	0.07	0.17	0.22	0.43	0.17	0.12	0.06	0.04	0.00
NA-20	32.5925	0.3137	0.68	0.12	0.17	0.33	0.43	0.75	0.31	0.26	0.12	0.06	0.00
Normalised root mean square error (NRMSE)									**0.433**	**0.281**	**0.152**	**0.120**	**0.144**
Mean absolute error (MAE)									**0.339**	**0.261**	**0.160**	**0.128**	**0.163**
Nash–Sutcliffe Efficiency Index (NSE)									**0.559**	**0.709**	**0.841**	**0.876**	**0.856**

0.152 and 0.120, 0.144 for *T25*, *T50* and *T100* return periods, respectively. The computed MAE values were 0.160, 0.128 and 0.163 for the *T25*, *T50* and *T100* return periods, respectively. Given that the NRMSE and MAE values are close to 0 and the NSE values are close to 1, the model validation results suggest that the accuracy of the developed coupled 1D–2D model was relatively high. The computed minimum NRMSE and MAE values and maximum NSE value suggest that the observed maximum flood depths were attributed to *T50* extreme rainfall events.

The study results have demonstrated that in the absence of simultaneously measured rainfall and flow data for an existing UDS, model accuracy of a coupled 1D–2D model can be ascertained through measurement of observed maximum flood depths at selected georeferenced flood hot spot locations. Model validation can also be undertaken using more recent citizen science approaches which utilise user-contributed photos and videos of flooded streets to estimate flood depths during extreme flooding events and to support the optimisation and selection of flood evacuation routes for emergency services (Alizadeh *et al.* 2022).

The study results have also demonstrated that the use of local sensitivity analysis (refer to Supplementary Information, Section 2.5) to identify the most sensitive model parameters, coupled with the use of high resolution Digital Elevation Models, and satellite imagery can significantly improve the accuracy of the developed urban flood models (Reinstaller *et al.* 2022). For future research, citizen science approaches for the validation of urban flood models in developing country cities are recommended (Alizadeh *et al.* 2022).

3.2. Effect of climate change on urban rainfall

3.2.1. Local intensity downscaling of urban rainfall

In this study, a minimum value of 1 mm/day was considered as the baseline to differentiate between wet and dry days. The results of the computed number of rainfall days (and their corresponding threshold values) and the correction factors for rainfall are presented in Tables 4 and 5, respectively, for the downscaled NorESM2-MM and GFDL-ESM4 global climate models.

Low threshold values (<1 mm) imply that within that month, the projected rainfall intensity and frequency were low as compared to threshold values above 1 mm.

Furthermore, the computed monthly correction factors were positive for all considered GCMs which suggests an increase in the projected future rainfall for Kampala. For the NorESM2-MM GCM, June and August are expected to be the wettest months, with factors exceeding four, while May and October will be the driest, with factors below 1.5. Similarly, for the GFDL-ESM4 GCM, July and August will be the wettest months, with factors over four, while May, October, and November will be the driest, with factors less than 1.0. Nonetheless, it is important to note that even during the driest months, there will still be an increase in rainfall intensity compared to the current climate conditions.

Table 4 | Calculation of the number of rainy days for each GCM

			Threshold (mm)	
Month	Observed average no. of rainfall days	Raw historical GCM average no. of rainfall days	NorESM2 -MM	GFDL-ESM4
1	9.83	9.83	0.68	0.35
2	8.25	8.25	0.44	1.37
3	14.00	14.00	1.07	1.40
4	16.63	16.63	2.43	4.98
5	14.21	14.21	1.36	4.76
6	9.63	9.63	0.03	1.06
7	9.17	1.21	1.00	0.22
8	12.88	12.88	0.04	0.29
9	15.13	15.13	0.25	1.22
10	18.33	18.33	2.03	4.42
11	16.13	16.13	3.74	6.47
12	11.54	11.54	3.38	1.82

Table 5 | Calculation of correction factors for rainfall

		NorESM2 -MM		GFDL-ESM4	
Month	Obs	Raw	Factor	Raw	Factor
1	7.98	4.24	2.24	3.45	2.58
2	7.88	3.19	2.86	5.92	1.73
3	10.27	5.87	2.14	9.78	1.23
4	10.50	9.30	1.53	16.43	0.92
5	8.03	6.87	1.46	12.76	1.00
6	7.24	1.49	4.94	3.65	2.80
7	7.36	4.99	1.85	1.72	4.90
8	9.60	2.24	4.36	2.52	4.30
9	9.90	4.56	2.30	5.03	2.60
10	9.35	9.17	1.31	13.88	0.99
11	10.99	10.72	1.58	17.97	0.96
12	7.88	8.23	1.63	8.81	1.13

3.2.2. Analysis of future climate change impacts on urban rainfall

The study results show that for all assessed GCMs, the medium emission scenario (SSP 2-4.5) led to smaller increases in daily rainfall compared to the severe emission scenario (SSP 5-8.5). The results further suggest that for both SSP 2-4.5 and SSP 5-8.5 climate change scenarios, the climate change factors are greater than 1 suggesting a general increase in rainfall intensity and duration in Kampala (Table 6).

Furthermore, for the SSP5-8.5 scenario, considerable variability was observed within the downscaled GCM model results. Specifically, the BCC-CMC-MR and IPSL-CM6A-LR GCMs resulted in the highest increase in daily rainfall of 116 and 116%, respectively, while the NorESM2-MM, MRI-ESM2-0 and GFDL-ESM4 GCMs resulted in moderate increases of 11, 33 and 44%, respectively. Furthermore, future climate projections for the SSP 2-4.5 scenario resulted in increases in rainfall that varied from 8 to 95% (Table 6).

The IPSL-CM6A-LR and BCC-CMC-MR GCMs resulted in relatively high change factors when compared to other GCMs and published climate change factors for Uganda (Ngoma *et al.* 2021) and hence were excluded from subsequent analysis. After the exclusion of the aforementioned GCMs, the GCMs with the lowest and highest change factors, namely NorESM2-MM and GFDL-ESM4, were selected for further investigation to ensure that the band of uncertainty is represented in the simulated urban flooding impact indicators.

Using the results of statistical downscaling, annual maximum daily rainfall values for each future year were derived (refer to Supplementary Information, Tables S1 and Table S2) and new design storms were developed for the near future period (2020–2049) considering a return period of 10 years (Figure 4).

Table 6 | Computed climate change factors for downscaled daily rainfall for selected GCMs

GCM	Modelling centre	Scenario	Computed Climate Change factor
GFDL-ESM4	Geophysical Fluid Dynamics Laboratory	SSP 2-4.5	1.24
		SSP 5-8.5	1.44
BCC-CMC-MR	Beijing Climate Center	SSP 2-4.5	1.98
		SSP 5-8.5	2.16
IPSL-CM6A-LR	Institut Pierre-Simon Laplace	SSP 2-4.5	1.95
		SSP 5-8.5	2.16
NorESM2-MM	Norwegian Climate Centre	SSP 2-4.5	1.08
		SSP 5-8.5	1.11
MRI-ESM2-0	Meteorological Research Institute (MRI)	SSP 2-4.5	1.10
		SSP 5-8.5	1.33

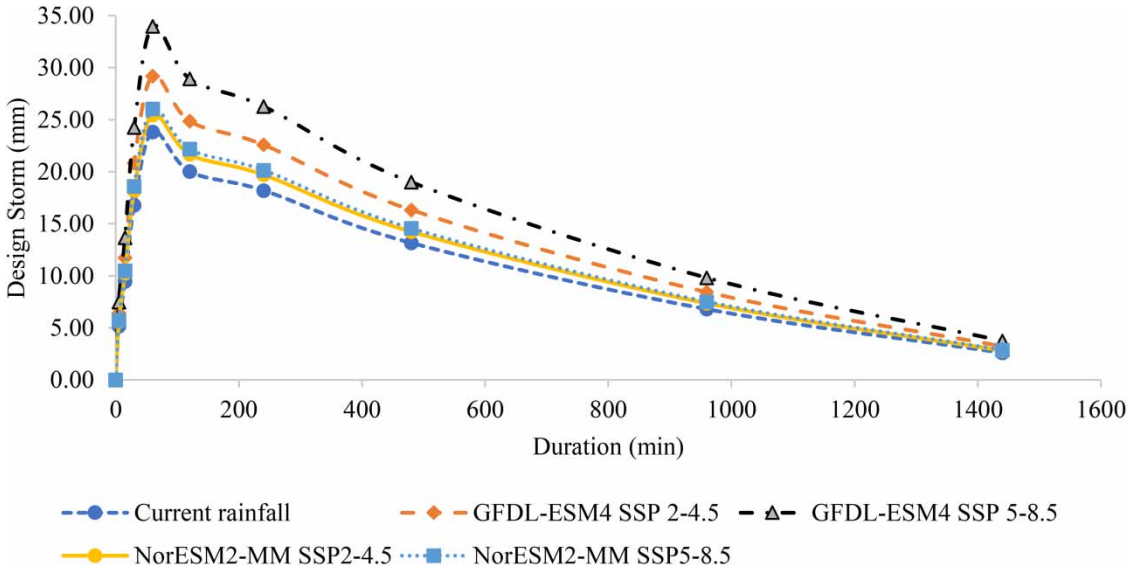

Figure 4 | Extracted design storms considering the projected future climate change conditions.

The study results suggest that future climate change will lead to 8–24% and 11–44% increase in daily rainfall intensities for the SSP2-4.5 and SSP5-8.5 scenarios, respectively. In previous studies, a current climate change factor of 1.2 has been applied to upscale rainfall for Kampala prior to undertaking detailed urban flood modelling studies (GIZ 2022). These results suggest that new climate change factors that range from 1.24 to 1.44 should be used to upscale observed rainfall for the near future period (2020–2049) to facilitate a more accurate assessment of flood risk in Kampala. The study results can facilitate a more accurate evaluation of potential climate change adaptation options, which is vital for enhancing the resilience of existing UDSs. In future research, the effect of land use change caused by rapid urbanisation, urban creep, and inner city densification should be investigated to provide a more wholistic picture of the projected future flooding impacts in Kampala.

3.3. UDS performance under current climate conditions and varying UDS initial states

The results of the coupled 1D–2D modelling for the existing Nakivubo UDS considering 'failed', 'partially-failed' and 'non-failed' UDS initial states are presented in Figures 5–7, respectively. The flood extent maps show that flooding is concentrated around the primary channels due to the prevailing topography that consists of gentle hills and narrow valleys where the existing UDSs are constructed. Furthermore, the study results show that the *T100* design rainstorm resulted in a 76.1% increase in flooding extent when compared to the *T2* design rainstorm under the 'failed' UDS initial state.

On the other hand, the *T100* design rainstorm resulted in a 33.6% increase in flooding extent when compared to the *T2* design rainstorm under the 'partially-failed' UDS initial state. Furthermore, the simulated flooding extents for all considered design storms for 'failed' UDS initial state were higher than the 'partially-failed' UDS initial state by 3–36.1%. However, the proportion of flood depths greater than 0.5 m was higher for the 'partially-failed' UDS initial state (44.8–74.3%) when compared to the 'failed' UDS initial state (38.4–54.3%). Furthermore, the results suggest that the 'non-failed' UDS initial state leads to a reduction of flooding extent of 5.7–28.8% when compared to 'failed' UDS initial state results (refer to Supplementary Information, Table S4).

These results confirmed that complete failure of the 1D-minor system is the 'worst-case' UDS initial state that is characterised by pipe failures, collapse of open channel sections, blockages, deposition of silt and sediment and the presence of vegetation significantly. This state reduces the system's ability to convey storm water flows, leading to more severe and widespread flooding even in cases where the initial UDS design capacity might otherwise convey the flows resulting from a given design rainfall event. The model results also indicate that regular cleaning, maintenance, and monitoring are critical to minimise internal system failures and to minimise pluvial flooding.

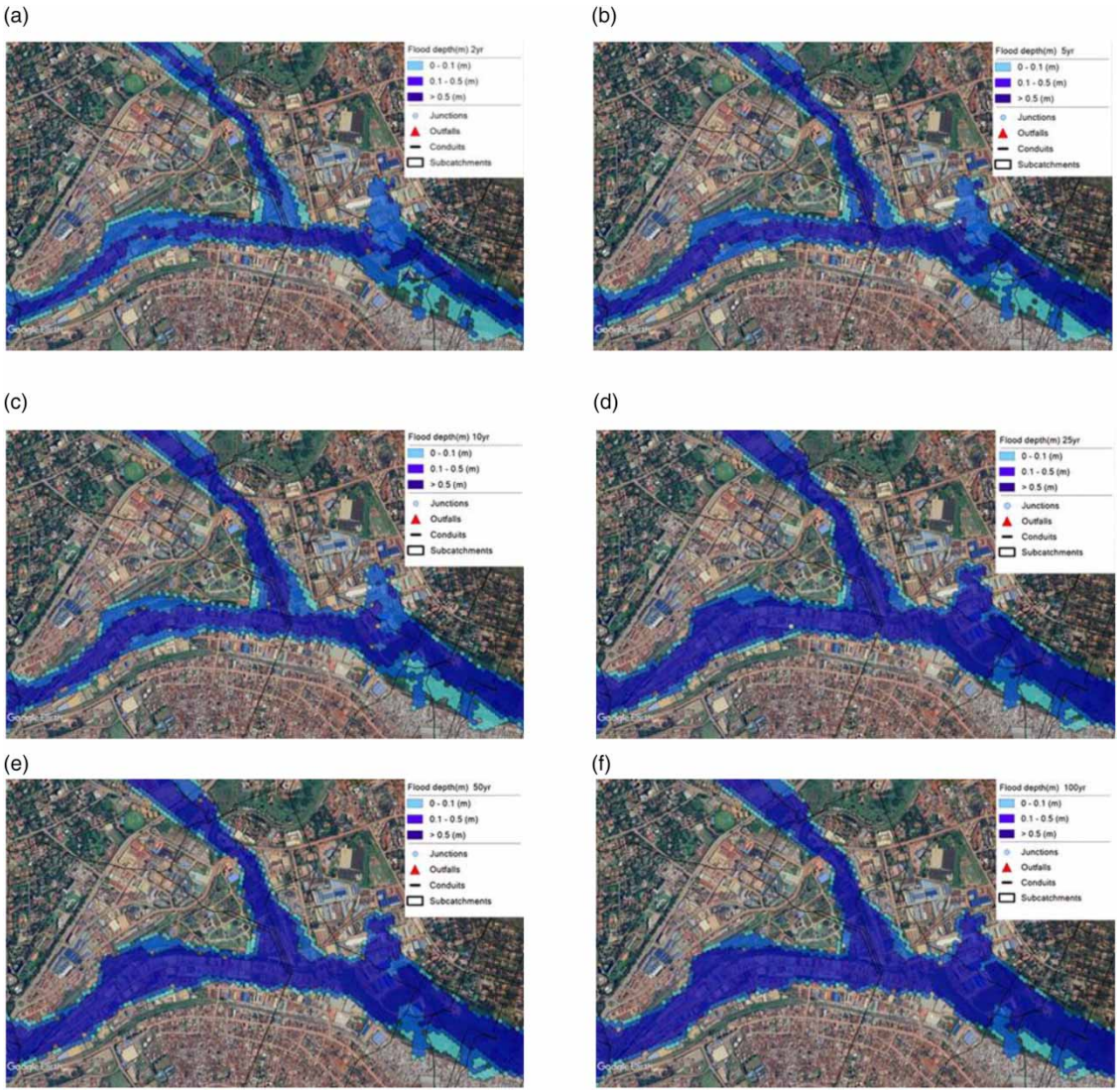

Figure 5 | Simulated flooding extent (flooded area) for the existing Nakivubo UDS considering the 'failed' initial UDS state and current climate conditions considering various return periods: (a) *T2*; (b) *T5*; (c) *T10*; (d) *T25*; (e) *T50 and (f) T100.*

3.4. UDS performance under future climate conditions and varying UDS initial states

The results of the coupled 1D–2D modelling for the existing Nakivubo UDS considering a 'failed', 'partially-failed' and 'non-failed' UDS initial states under the projected future climate change are presented in Figures 8–10, respectively. The study results for the 'failed' UDS initial state suggest that future climate change considering the *T10* design storm will increase the flooding extent by 2.8–14.8% for the SSP2-4.5 scenario. On the other hand, the *T10* design storm increased flooding extent by 5.0–29.9% considering SSP5-8.5 severe forcing scenarios. These results also indicate that considering the worst-case scenario (GFDL-ESM4, SSP5-8.5), a *T10* design storm under projected future climate change will lead to a similar increase in flooding extent as a *T100* year design storm under the current climate conditions.

In addition, the study results for the 'partially-failed' UDS initial state suggest that future climate change considering the *T10* design storm led to a slightly lower increase in flooding extent of 4.4–8.9% for SSP2-4.5 scenarios. On the other hand, the *T10* design storm resulted in a 16.2–17.4% increase in the resulting flooding extent considering the SSP 5-8.5 severe forcing scenarios. Similar to the 'failed' UDS initial state, the results for the 'partially-failed' UDS initial state also indicate that considering the worst-case scenario (GFDL-ESM4 (SSP5-8.5)), a *T10* design storm under projected future climate change will result in a similar flooded area as a *T100* year design storm under the current climate conditions.

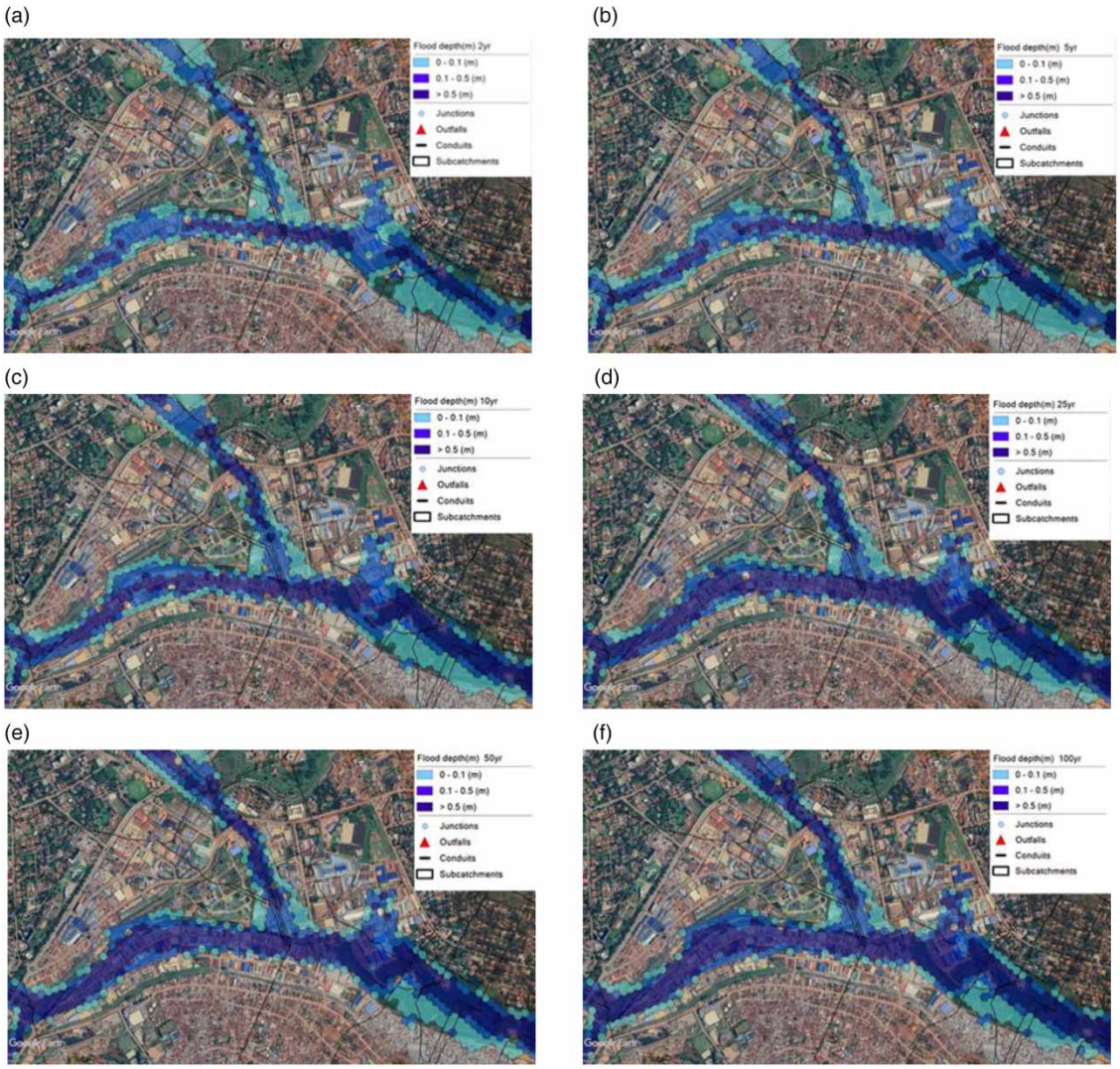

Figure 6 | Simulated flooding extent (flooded area) for the existing Nakivubo UDS considering the 'partially-failed' UDS initial state and current climate conditions considering various return periods: (a) *T2*; (b) *T5*; (c) *T10*; (d) *T25*; (e) *T50 and (f) T100.*

On the other hand, the study results for the 'non-failed' UDS initial state suggest that future climate change considering the *T10* design storm led to a slightly lower increase in flooding extent of 4.3–9.3% for the SSP2-4.5 scenario. On the other hand, the *T10* design storm resulted in a 13.7–14.8% increase in the resulting flooding extents considering the SSP 5-8.5 severe forcing scenarios. The results for the 'non-failed' UDS initial state indicate that considering the worst-case scenario (GFDL-ESM4 (SSP5-8.5)), a *T10* design storm under projected future climate change will lead to result in a similar flooded area as a *T50* year design storm under the current climate conditions (refer to Supplementary Information, Table S5).

It should be noted that the primary and secondary drainage systems in Kampala were designed considering *T10* and *T2* design storms, respectively. The study results have therefore demonstrated that the current hydraulic conveyance capacity of the Nakivubo UDS is insufficient to handle the current *T2* flows and that compound climate change and internal system failure threats will significantly increase flood risk, as the UDS hydraulic capacity is pushed beyond limits more frequently. Furthermore, by incorporating climate projections in urban drainage modelling, this research has demonstrated how future climate change exacerbates the impacts of internal UDS failures and points to the need for cities to prepare for higher flood risk thresholds in the future. The results have also demonstrated that improvement in UDS cleaning and maintenance practices could reduce the projected flooding extent by up to 5.5 and 15.1% for the SSP2-4.5 and SSP5-8.5 scenarios, respectively.

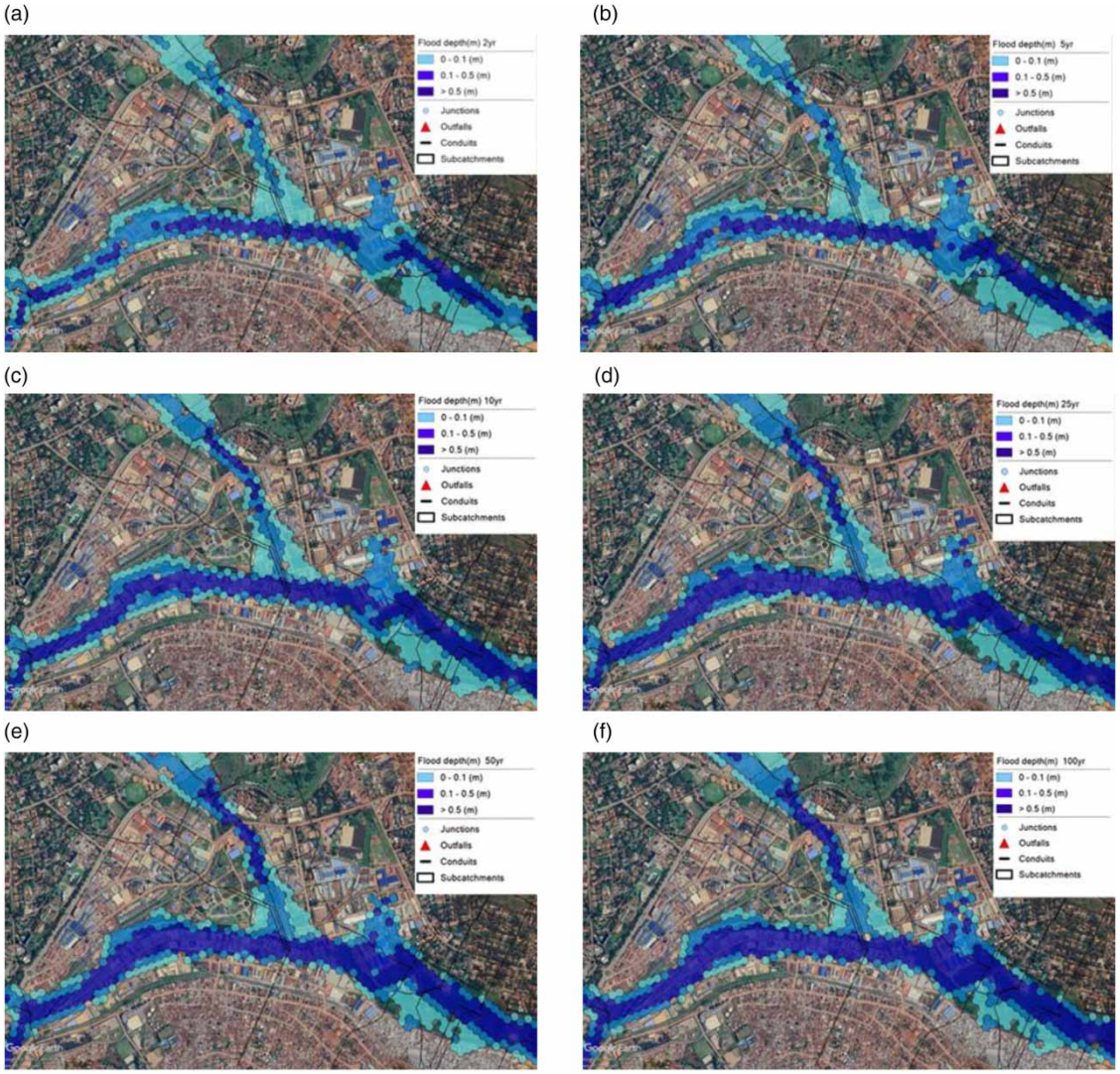

Figure 7 | Simulated flooding extent (flooded area) for the existing Nakivubo UDS considering the 'non-failed' UDS initial state and current climate conditions. Blue colour is the inundated area and the red mark is the outlet: (a) *T2;* (b) *T5;* (c) *T10;* (d) *T25*; (e) *T50 and (f) T100.*

3.5. Effectiveness of modelled BGI options under current climate conditions

The results for the 'failed' UDS initial state suggest that the use of infiltration trenches leads to an average reduction in total flood volume of 18.2% [11.8–29.8%] under current climate conditions. On the other hand, the use of bioretention cells leads to an average reduction of total flood volume of 12.2% [7.9–19.8%] (Figure 11). The use of spatially distributed RWH tanks led to an average reduction in total flood volume of 11.1% [7.2–17.8%]. The results further indicated that RWH, infiltration trenches and bioretention cells led to a very low reduction in average flood duration of 8.9, 4.8 and 5.1%. However, for the *T2* design rainstorm, infiltration trenches and bioretention cells lead to a minimal increase in the average flood duration of 4.5 and 1.5%, respectively. Further investigation showed that the average flood duration was computed for only 15 flooded nodes, which resulted in higher average values when compared to the corresponding values for higher return periods with a higher number of flooded nodes that is: *T5* (24 flooded nodes), *T10* (39 flooded nodes), *T25* (47 flooded nodes), *T50* (51 flooded nodes) and *T100* (55 flooded nodes).

Furthermore, the results for the 'partially-failed' UDS initial state suggest that the use of infiltration trenches leads to 18.7% [12.0 - 31.6%] reduction in total flood volume. The use of bioretention cells and spatially distributed RWH tanks led to an average reduction of total flood volume of 12.5% [8.0–21.0%] and 11.4% [7.3–19.2%], respectively (Figure 12). The results further indicated that RWH tanks, infiltration trenches and

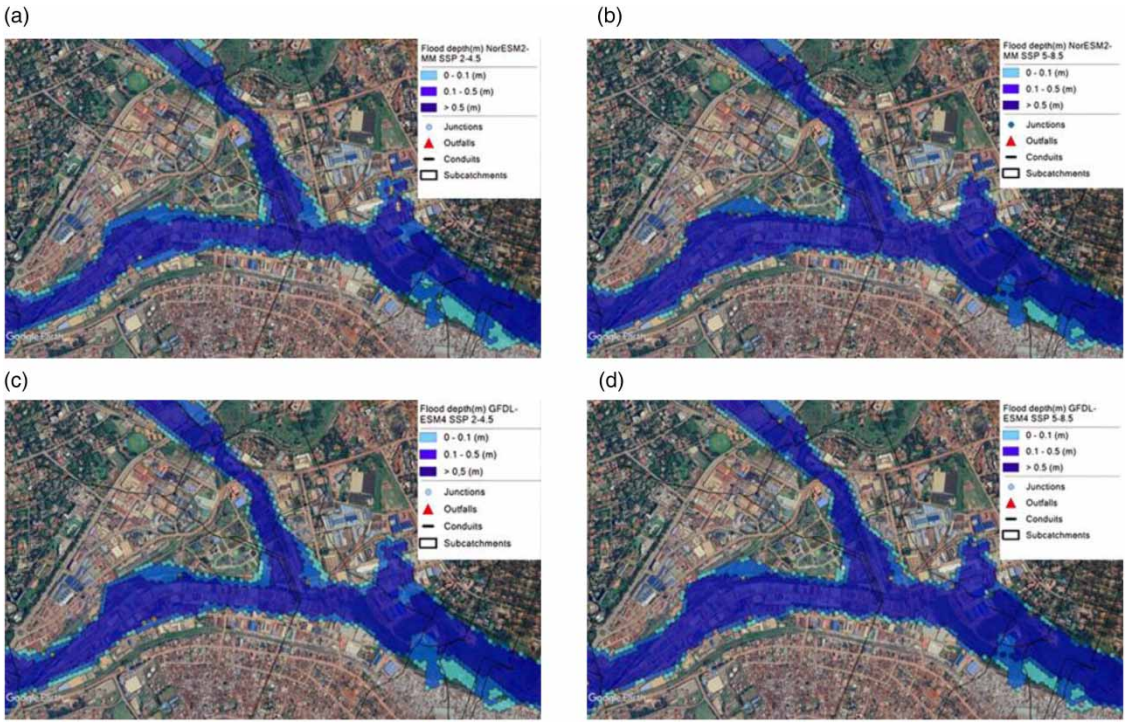

Figure 8 | Simulated flooding extent (flooded area) for the existing Nakivubo UDS considering the 'failed' initial state and projected T10 future climate change conditions: **(a)** NORESM2 SSP2-4.5; **(b)** NORESM2 SSP 5-8.5 **(c)** GFDL SSP2-4.5 and **(d)** GFDL SSP 5-8.5 scenarios.

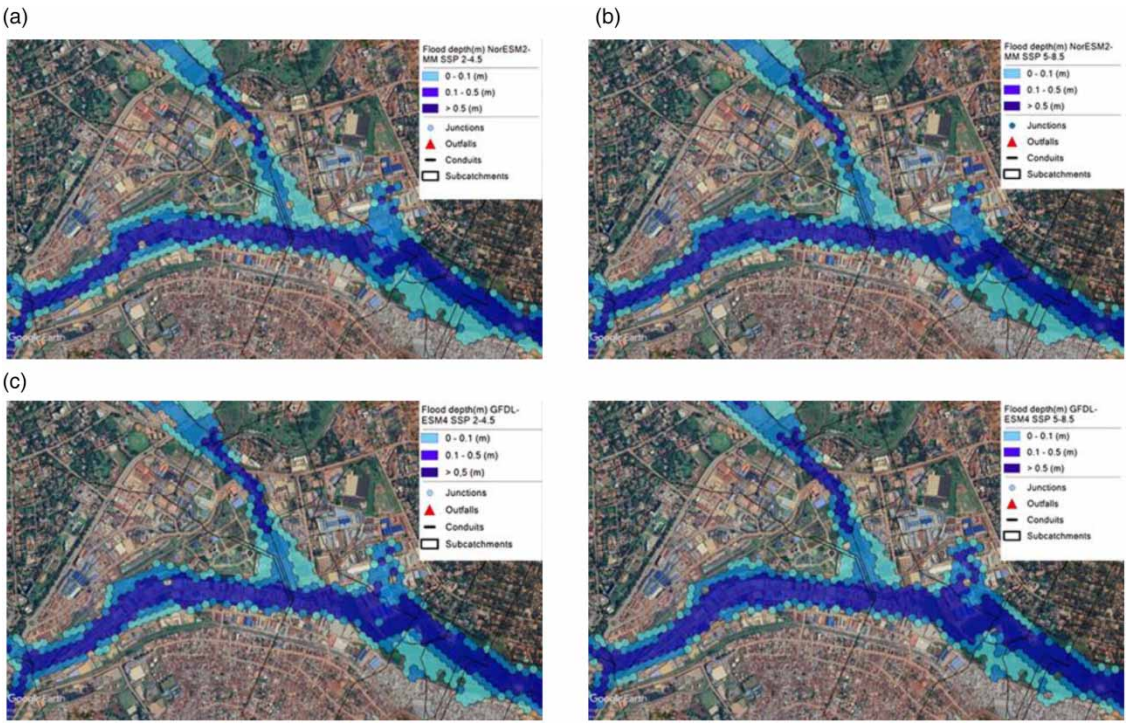

Figure 9 | Simulated flooding extent (flooded area) for the existing Nakivubo UDS considering the 'partially-failed' initial state and projected T10 future climate change conditions: (a) NORESM2 SSP2-4.5; (b) NORESM2 SSP 5-8.5 (c) GFDL SSP2-4.5 and (d) GFDL SSP 5-8.5 scenarios.

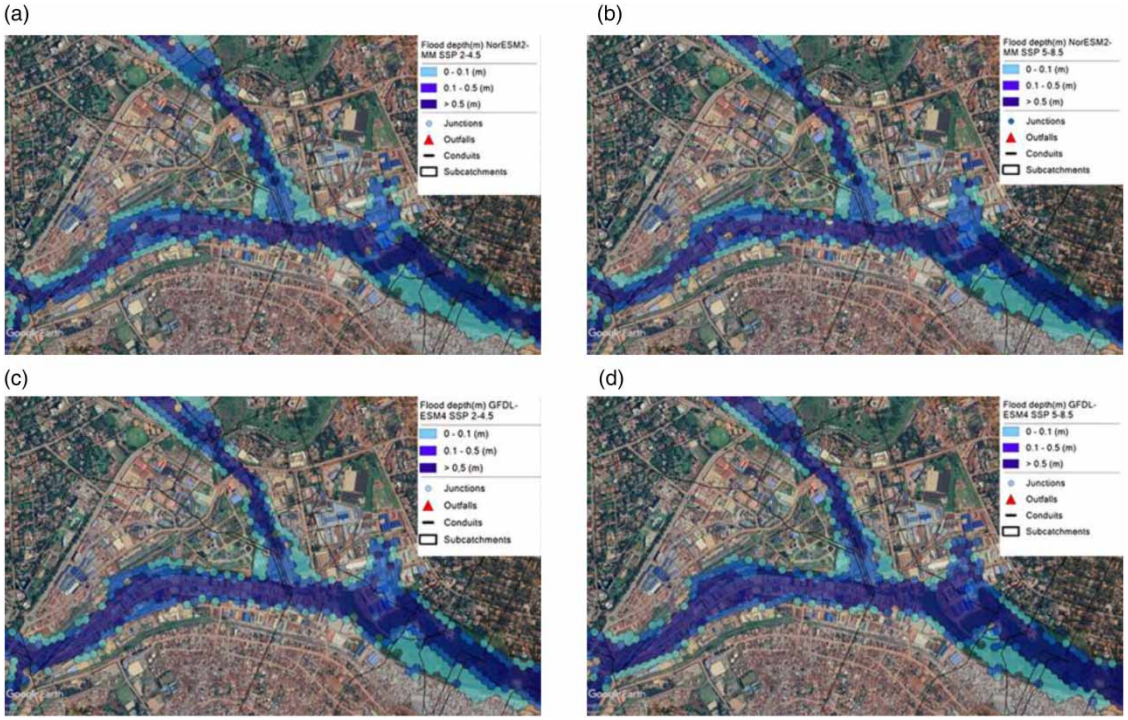

Figure 10 | Simulated flooding extent (flooded area) for the existing Nakivubo UDS considering the 'non-failed' state and projected T10 future climate change conditions. Blue colour is the inundated area and the red mark is the outlet: (a) NORESM2 SSP2-4.5; (b) NORESM2 SSP 5-8.5; (c) GFDL SSP2-4.5 and (d) GFDL SSP 5-8.5 scenarios.

bioretention cells resulted in a minimal reduction of the average flood duration of 10.2, 10.9 and 6.5%, respectively.

On the other hand, the results for the 'non-failed' UDS initial state suggest that the use of infiltration trenches leads to an average reduction in total flood volume of 19.9% [14.1–30.1%]. The use of bioretention cells and spatially distributed RWH tanks leads to an average reduction of total flood volume of 14.2% [10.3–20.6%] and 12.9% [9.4–18.6%], respectively. The results further indicated that RWH tanks, infiltration trenches and bioretention cells led to a more substantial reduction of 40.7, 28.6 and 27.1% in the average flood duration (Figure 13).

These results are in agreement with Panos *et al.* (2021) who concluded that the use of distributed bioretention cells in redeveloped areas can enable the existing UDS to convey additional storm water flows caused by 8.5–12.5% increase in effective rainfall prior to its failure. Furthermore, the study results agree with Mugume *et al.* (2024) and Webber *et al.* (2020) who concluded that BGI can effectively minimise flooding caused by low to moderate rainfall events (Mugume *et al.* 2024), leaving substantial residual flood risk when more extreme rainfall events occur. This, therefore, necessitates a paradigm shift from the implementation of singular BGI options to consideration of integrated grey-blue-green infrastructure (IGBGI) in which investment in spatially distributed BGI is complemented with rehabilitation or expansion of existing grey infrastructure leading to enhancement of global UDS resilience to flooding and co-benefits that include the provision of alternative water supplies, reduction of urban heat island effect and improvement of storm water quality (Alves *et al.* 2020; Webber *et al.* 2020; Wang *et al.* 2023).

3.6. Effectiveness of modelled BGI options under future climate change conditions

Model simulations considering a 'failed' UDS initial state were undertaken using the projected *T10* design rainstorms. The results suggest that the use of bioretention cells led to an average reduction of total flood volume of 9.8% [7.4–11.8%]. The results further suggest that the use of infiltration trenches and spatially distributed RWH tanks led to an average reduction in total flood volume of 14.6% [11.1–17.6%] and 8.9% [6.8–10.8%], respectively. Considering the duration of flooding, the results indicate that RWH, infiltration trenches and bioretention cells led to a minimal reduction in the average flood duration of 7.4, 6.8 and 1.3%, respectively (Figure 14).

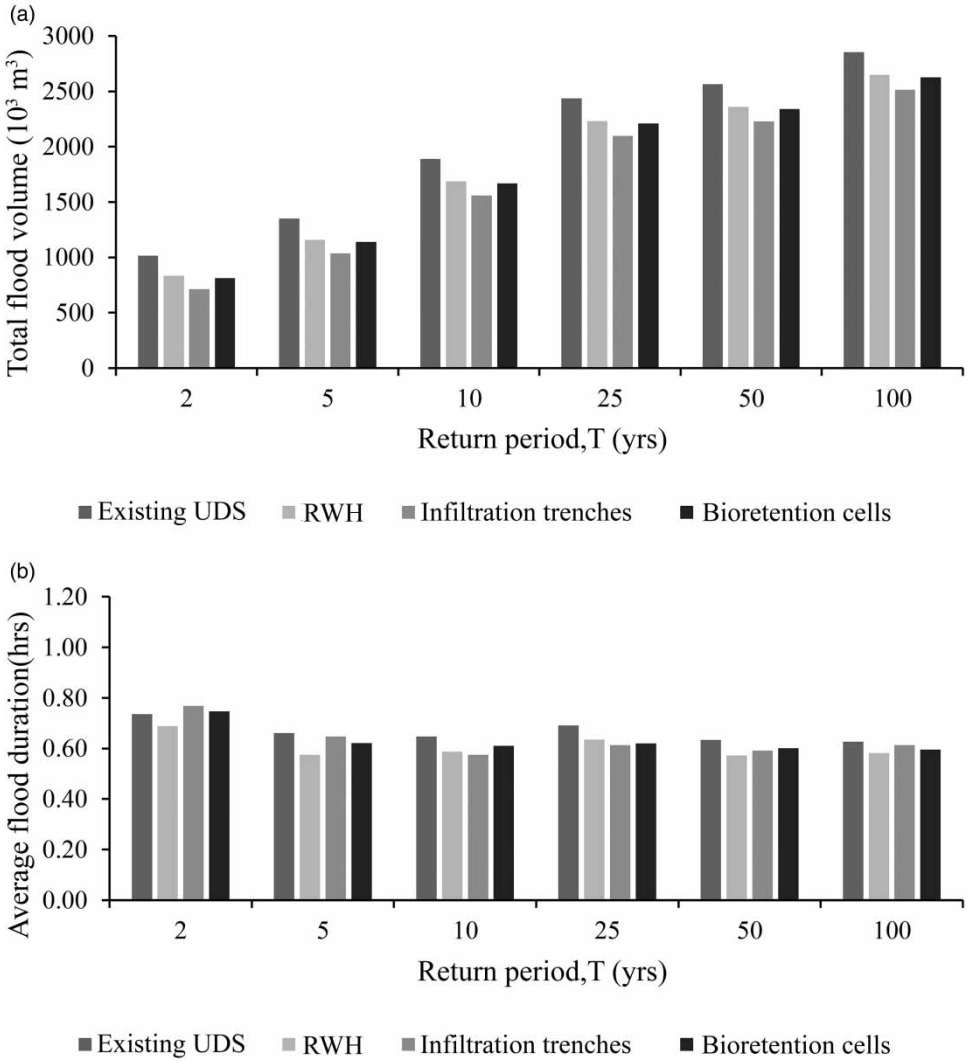

Figure 11 | BGI effect on reduction of (a) total flood volume (top) and average flood duration (bottom) for 'failed' UDS initial state condition.

Furthermore, model simulations considering a 'partially-failed' UDS state were undertaken using the projected *T10* design rainstorms. The results suggest that the use of bioretention cells led to an average reduction of total flood volume of 9.8% [7.4–11.8%]. The results further suggest that the use of infiltration trenches and spatially distributed RWH tanks led to an average reduction in total flood volume of 14.6% [11.1–17.6%] and 8.9% [6.8–10.8%], respectively. Considering the duration of flooding, the results indicate that RWH, infiltration trenches and bioretention cells led to a minimal reduction in the average flood duration of 6.7, 4.0 and 1.9%, respectively (Figure 15).

The model simulation results for the 'non-failed' UDS initial state suggest that the use of bioretention cells led to an average reduction of total flood volume of 12.2% [9.8–14%]. The results further suggest that the use of infiltration trenches and spatially distributed RWH tanks led to an average reduction in total flood volume of 16.8% [13.4–19.3%] and 11.2% [9.1–12.9%], respectively. Considering the duration of flooding, the results indicate that RWH, infiltration trenches and bioretention cells led to more than 34.3% reduction in the average flood duration (Figure 16).

The study results suggest that future climate change and internal UDS failures significantly reduce the performance of all considered BGI options which is in agreement with Neumann *et al.* (2024). These results also agree with Zhang (2024) who concluded that optimally located spatially distributed green infrastructure led to a low reduction of peak flows of 3.3–18% under future climate change in Guangzhou, China. Furthermore, the study results have demonstrated that appropriately designed infiltration-based systems led to more significant flood

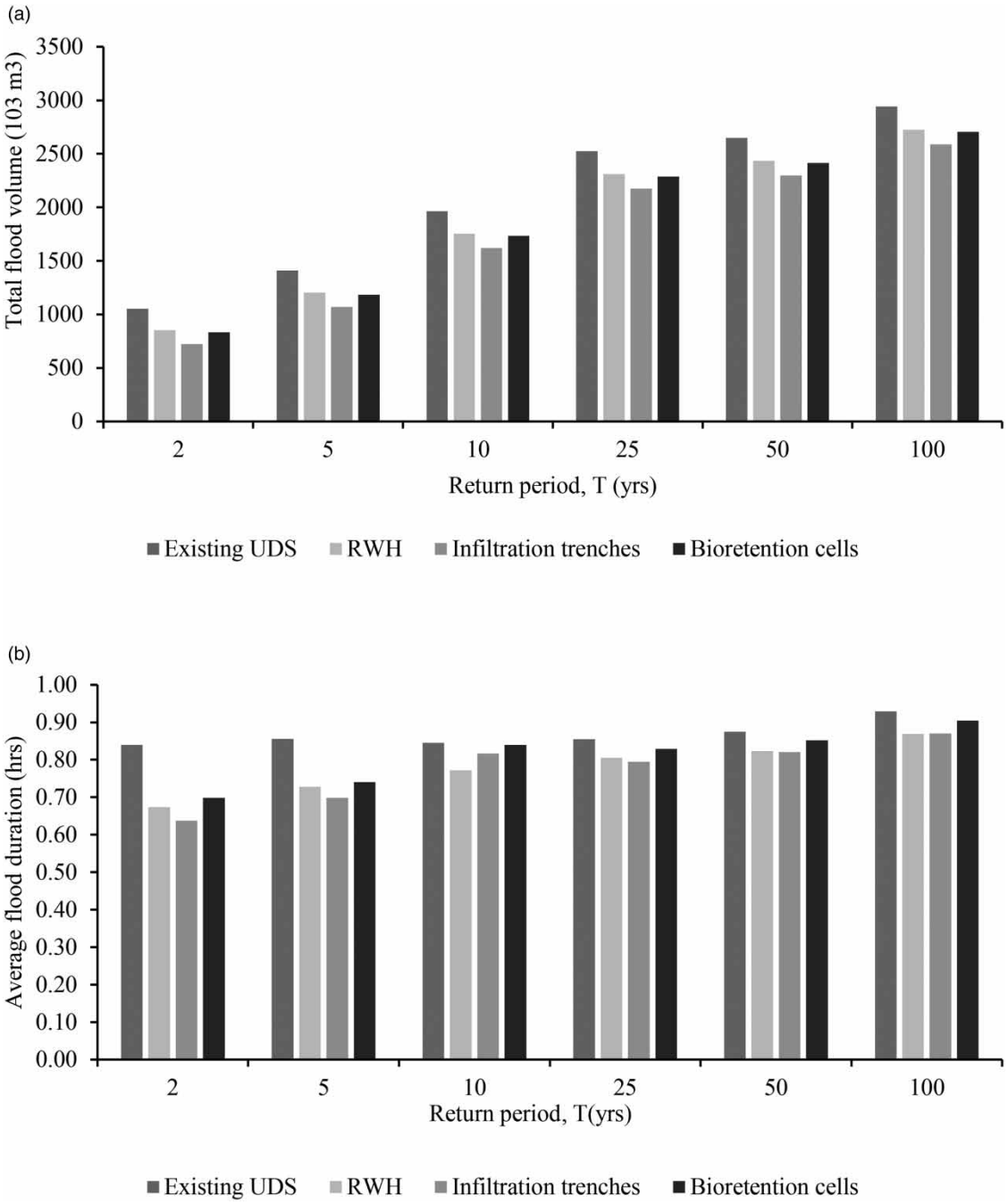

Figure 12 | BGI effect on reduction of (a) total flood volume (top) and average flood duration (bottom) for the 'partially-failed' UDS initial state condition.

reduction benefits during extreme rainfall (Neumann *et al.* 2024). However, further research using pilot studies is required to determine optimal design parameters (hydraulic conductivity, porosity, void ratio, seepage rate) for infiltration-based systems which are influenced by the choice of design parameters and prevailing sub-surface soil conditions in various cities (Neumann *et al.* 2024).

In addition, the study results suggest that although spatially distributed RWH tanks were more effective when compared to infiltration-based systems under current climate conditions (Mugume *et al.* 2024), the additional hydraulic loading caused by climate change induced extreme rainfall significantly reduced their effectiveness. Improving the effectiveness of RWH systems for urban flood reduction effectiveness would require the tanks to be equipped with passive or more advanced active control systems for the regulated release of rainwater to

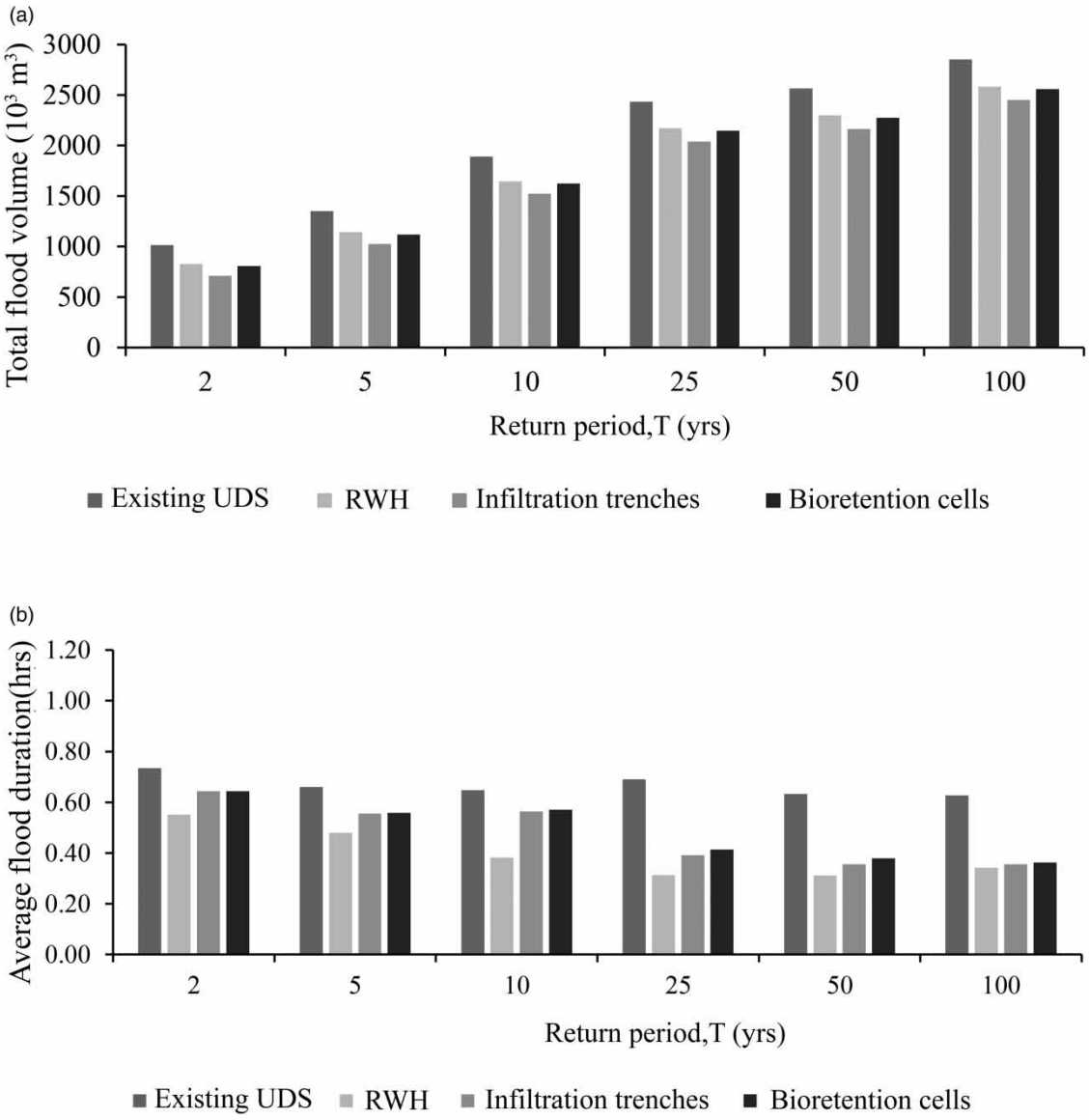

Figure 13 | BGI effect on reduction of (a) total flood volume and (b) average flood duration for 'non-failed' UDS initial state.

the UDS to ensure that an adequate storm water control volume is maintained in the tanks prior to the subsequent rainfall event (Mugume *et al.* 2017).

4. CONCLUSIONS

This research focused on the evaluation of effectiveness of BGI in the reduction of pluvial flooding provides a rigorous characterisation of the potential of BGI in enhancing the resilience of UDSs experiencing compound climate change and internal system failure threats. A methodology that combined local intensity downscaling of five CMIP6 Global Climate Models (GCMs) for projection of future rainfall, coupled with 1D–2D urban drainage modelling and internal system failure modelling was developed. The developed methodology was applied to investigate the performance of BGI options for the reduction of pluvial flooding, using a case study of the Nakivubo UDS which drains a highly urbanised catchment in Kampala, Uganda. Based on the study findings, the following conclusions can be made:

(a) **2D surface flow modelling and visualisation:** The adopted coupled 1D–2D modelling approach provided valuable visual representations of 2D flood extents and depths in the case study catchment. The study also revealed the need to use multiple GCMs to ensure that uncertainty in climate modelling results is accounted

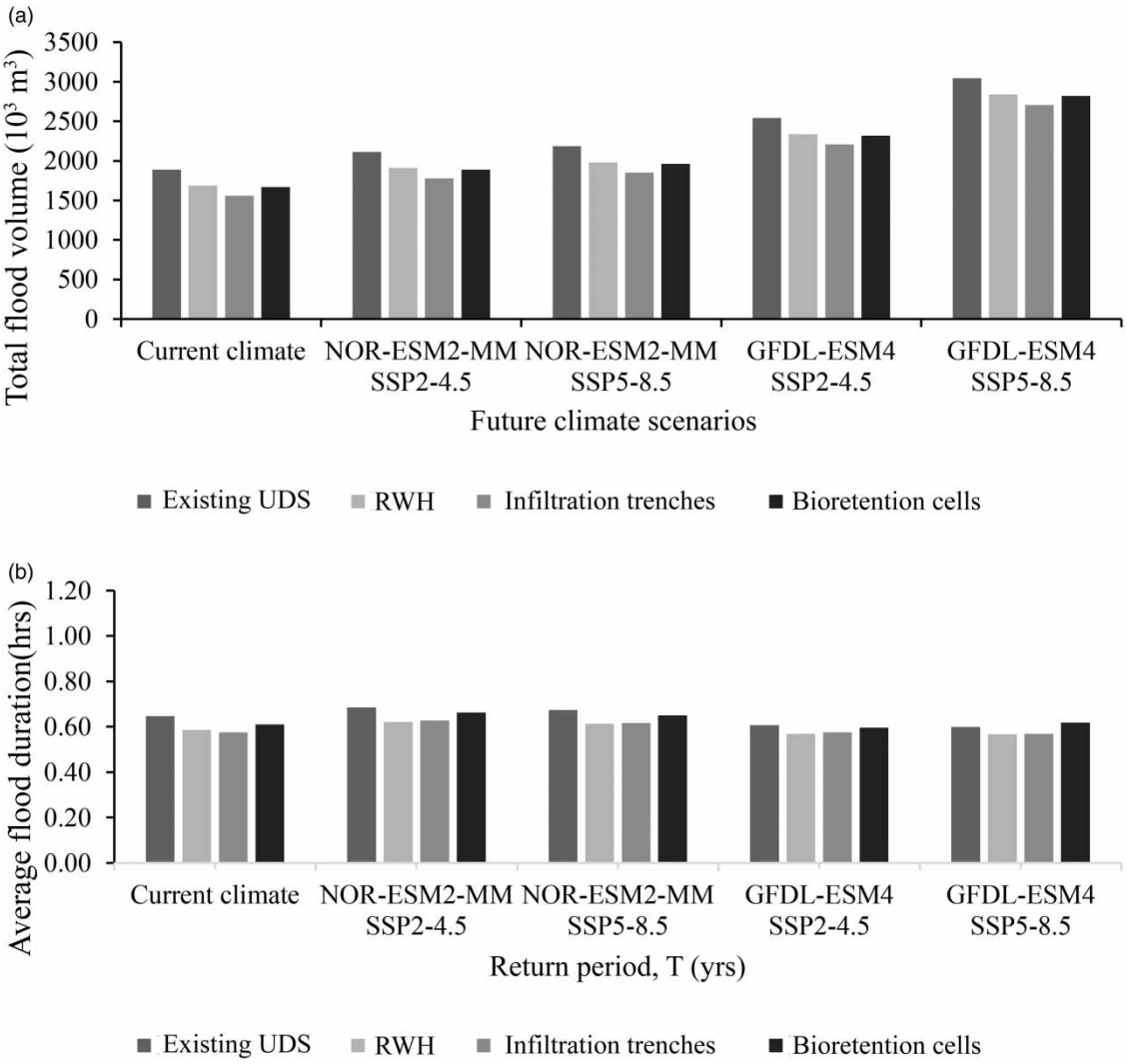

Figure 14 | BGI effect on reduction of (a) total flood volume and (b) average flood duration for 'failed' UDS initial state.

for in the 2D surface flow modelling. This approach can support engagement with local communities and key stakeholders and can facilitate co-creation of context-specific adaptation strategies that can be implemented by city authorities, property developers and other flood risk management stakeholders to enhance resilience to flooding.

(b) **UDS performance under internal system failures**: The study has demonstrated that BGI provides secondary flood mitigation benefits in situations where existing UDSs experience internal system failures caused by blockages, pipe, pump and sensor failures, power outages, structural collapse of drainage channel sections, deposition of sediments and solid waste. The study findings suggested that the hydraulic conveyance capacity of the existing Nakivubo UDS in Kampala is inadequate to safely convey storm water runoff resulting from the projected future rainstorms. The study findings also suggested that implementation of spatially distributed BGI at urban catchment scale reduces reliance on centralised UDSs thereby providing multiple layers of flood protection, which is crucial for maintaining UDS functionality during failure conditions.

(c) **Resilience under climate change:** The study has demonstrated that climate change will increase the frequency of occurrence of extreme rainfall in Kampala from 1 in 100 years to 1 in 10 years by 2050 which will exacerbate the urban flooding challenge in Kampala. This therefore creates the need to integrate BGI into urban planning to enhance existing UDS flexibility and redundancy attributes thereby enhancing the resilience of existing UDSs under a changed climate.

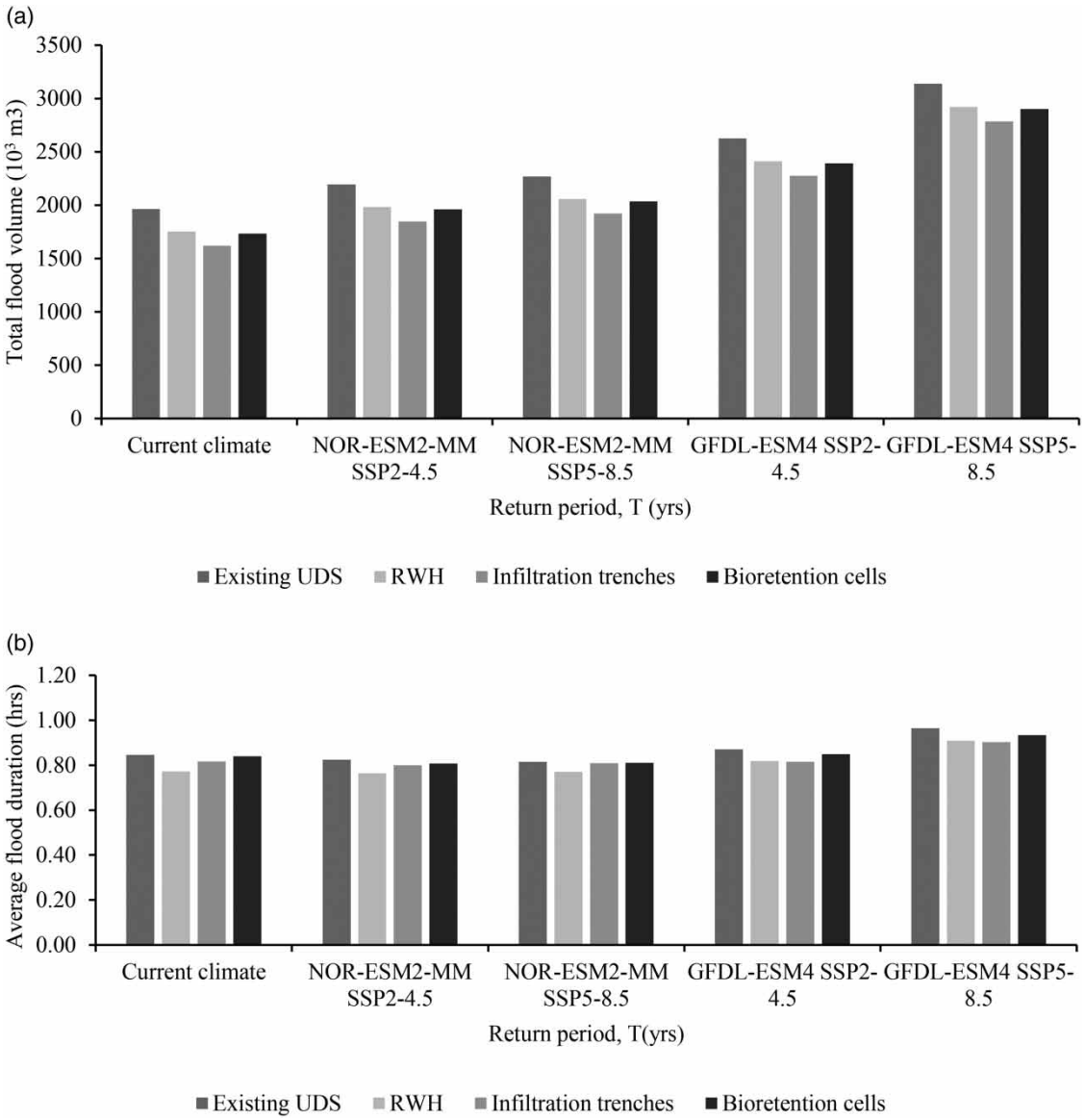

Figure 15 | BGI effect on reduction of (a) total flood volume (top) and (b) average flood duration (bottom) for 'partially-failed' UDS initial state condition.

(d) **Effectiveness of BGI:** The study has demonstrated that catchment scale implementation of spatially distributed infiltration trenches, bioretention cells and RWH systems leads to a modest reduction in flood mitigation benefits, suggesting that BGI are only effective during the occurrence of low to moderate rainfall.

Based on the study findings, it is concluded that for Kampala City, BGI should be integrated into urban planning policies and strategies to complement investments in improved asset management, rehabilitation and expansion of existing grey UDSs in order to provide cost-effective solutions towards resilient and sustainable storm water management. However, further research is needed to address challenges that include: (a) quantifying co-benefits and trade-offs in the implementation of BGI under different urban contexts and climate conditions (b) optimisation of scale and spatial distribution of BGI during integration with existing grey urban drainage infrastructure (c) improved modelling of 2D surface flows using recent 2D direct rainfall (rain-on grid) modelling approaches to better represent 2D surface flow interactions with the modelled BGI options and (d) development and application citizen science approaches for improved 2D surface flow model validation in data scarce environments using Citizen Science and Artificial Intelligence (e) implementation and monitoring of pilot scale bioretention cells and infiltration trenches to facilitate improved BGI model calibration and validation data collection in varying city contexts.

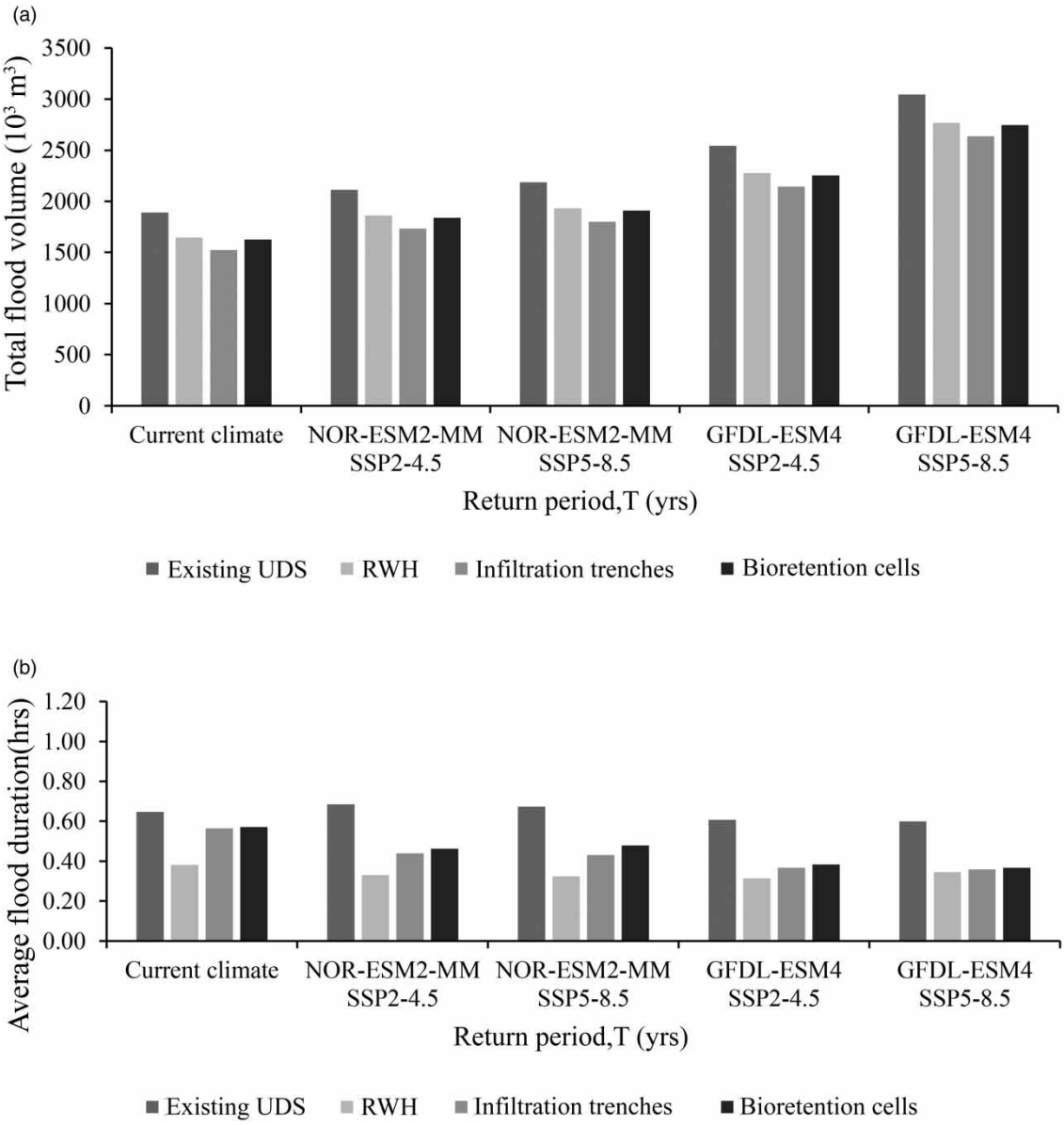

Figure 16 | BGI effect on reduction of (a) total flood volume and (b) average flood duration for 'non-failed' UDS initial state.

Finally, the novelty of this research lies in the application of a combination of a more complex coupled 1D–2D urban flood modelling approach and compound-threat analysis (consideration of future climate change and internal system failure scenarios) to investigate the effectiveness of BGI in enhancing the resilience of existing UDSs in cities. The adopted approach therefore enabled consideration of dynamic interactions between BGI elements and the urban water cycle under extreme climate and internal system failure conditions. Finally, the research has presented a new approach that is not considered in conventional urban drainage design and rehabilitation approaches.

ACKNOWLEDGEMENTS

We acknowledge the Directorate of Water Resources Management (DWRM), Ministry of Water and Environment, Uganda and Kampala Capital City Authority (KCCA) for provision of the datasets used in the study. Also, we acknowledge CHI Canada for providing us with the PCSWMM V 7.6 license used in this study. The insights of two anonymous reviewers are also gratefully acknowledged. We also confirm that there are no relevant financial or non-financial competing interests to report.

DATA AVAILABILITY STATEMENT

All relevant data are included in the paper or its Supplementary Information.

CONFLICT OF INTEREST

The authors declare there is no conflict.

REFERENCES

Akinsanola, A. A., Ongoma, V. & Kooperman, G. J. (2021) Evaluation of CMIP6 models in simulating the statistics of extreme precipitation over Eastern Africa, *Atmos. Res.*, **254**, 1–12. https://doi.org/10.1016/j.atmosres.2021.105509.

Alizadeh, B., Li, D., Hillin, J., Meyer, M. A., Thompson, C. M., Zhang, Z. & Behzadan, A. H. (2022) Human-centered flood mapping and intelligent routing through augmenting flood gauge data with crowdsourced street photos, *Adv. Eng. Inf.*, **54**, 1–12. https://doi.org/10.1016/j.aei.2022.101730.

Alves, A., Vojinovic, Z., Kapelan, Z., Sanchez, A. & Gersonius, B. (2020) Exploring trade-offs among the multiple benefits of green-blue-grey infrastructure for urban flood mitigation, *Sci. Total Environ.*, **703**, 1–14. https://doi.org/10.1016/j.scitotenv.2019.134980.

Arinabo, D. (2023) Reconciling multiple forms of flood risk knowledge and institutional responses: Insights from Kampala's flood management regime, *Int. J. Disaster Risk Reduct.*, **94**, 1–13. https://doi.org/10.1016/j.ijdrr.2023.103829.

Balbastre-Soldevila, R., García-Bartual, R. & Andrés-Doménech, I. (2019) A comparison of design storms for urban drainage system applications, *Water*, **11**, 1–15. https://doi.org/10.3390/w11040757.

Blanc, J., Hall, J. W., Roche, N., Dawson, R. J., Cesses, Y., Burton, A. & Kilsby, C. G. (2012) Enhanced efficiency of pluvial flood risk estimation in urban areas using spatial–temporal rainfall simulations, *J. Flood Risk Manag.*, **5**, 143–152. https://doi.org/10.1111/j.1753-318X.2012.01135.x.

Buontempo, C., Burgess, S. N., Dee, D., Pinty, B., Thépaut, J. N., Rixen, M., Almond, S., Armstrong, D., Brookshaw, A., Lopez, A. A., Bell, B., Bergeron, C., Cagnazzo, C., Comyn-Plat, E., Damasio-Da-Costa, E., Guillory, A., Hersbach, H., Horányi, A., Nicolas, J., Obregon, A., Ramos, E. P., Raoult, B., Muñoz-Sabate, J., Simmons, A., Soci, C., Suttie, M., Vamborg, F., Varndell, J., Vermoote, S., Yang, X. & De Marcilla, J. G. (2022) The copernicus climate change service: Climate science in action, *Bull. Am. Meteorol. Soc.*, **103**, E2669–E2687. https://doi.org/10.1175/BAMS-D-21-0315.1.

Butler, D., Digman, C., Makropoulos, C. & Davies, J. W. (2018) *Urban Drainage*, 4th edn. London and New York: CRC Press, Taylor and Francis Group.

Chitwatkulsiri, D., Miyamoto, H., Irvine, K. N., Pilailar, S. & Loc, H. H. (2022) Development and application of a real-Time flood forecasting system (RTFlood system) in a tropical urban area: A case study of Ramkhamhaeng Polder, Bangkok, Thailand, *Water*, **14**, 1–21. https://doi.org/10.3390/w14101641.

Digman, C. J., Anderson, N., Rhodes, G., Balmforth, D. J. & Kenney, S. (2014) Realising the benefits of integrated urban drainage models, *Water Manage.*, **167**, 30–37. https://doi.org/10.1680/wama.12.00083.

Djordjević, S., Prodanović, D. & Maskimović, C. (1999) An approach to simulation of dual drainage, *Water Sci. Technol.*, **39**, 95–103.

Djordjević, S., Prodanović, D., Maksimović, Č., Ivetić, M. & Savić, D. A. (2005) SIPSON – Simulation of interaction between pipe flow and surface overland flow in networks, *Water Sci. Technol.*, **52**, 275–283.

Dong, T. & Dong, W. (2021) Evaluation of extreme precipitation over Asia in CMIP6 models, *Clim. Dyn.*, **57**, 1751–1769. https://doi.org/10.1007/s00382-021-05773-1.

Dong, X., Guo, H. & Zeng, S. (2017) Enhancing future resilience in urban drainage system: Green versus grey infrastructure, *Water Res.*, **124**, 280–289. https://doi.org/10.1016/j.watres.2017.07.038.

Drosou, N., Soetanto, R., Hermawan, F., Chmutina, K., Bosher, L. & Hatmoko, J. (2019) Key factors influencing wider adoption of blue-Green infrastructure in developing cities, *Water*, **11**, 1–20.

Dunne, J. P., Horowitz, L. W., Adcroft, A. J., Ginoux, P., Held, I. M., John, J. G., Krasting, J. P., Malyshev, S., Naik, V., Paulot, F., Shevliakova, E., Stock, C. A., Zadeh, N., Balaji, V., Blanton, C., Dunne, K. A., Dupuis, C., Durachta, J., Dussin, R., Gauthier, P. P., Griffies, S. M., Guo, H., Hallberg, R. W., Harrison, M., He, J., Hurlin, W., McHugh, C., Menzel, R., Milly, P. C., Nikonov, S., Paynter, D. J., Ploshay, J., Radhakrishnan, A., Rand, K., Reichl, B. G., Robinson, T., Schwarzkopf, D. M., Sentman, L. T., Underwood, S., Vahlenkamp, H., Winton, M., Wittenberg, A. T., Wyman, B., Zeng, Y. & Zhao, M. (2020) The GFDL earth system model version 4.1 (GFDL-ESM 4.1): Overall coupled model description and simulation characteristics, *J. Adv. Model. Earth Syst.*, **12**, 1–56. https://doi.org/10.1029/2019MS002015.

Eyring, V., Bony, S., Meehl, G. A., Senior, C. A., Stevens, B., Stouffer, R. J. & Taylor, K. E. (2016) Overview of the coupled model intercomparison project phase 6 (CMIP6) experimental design and organization, *Geosci. Model Dev.*, **9**, 1937–1958. https://doi.org/10.5194/gmd-9-1937-2016.

Fang, G. H., Yang, J., Chen, Y. N. & Zammit, C. (2015) Comparing bias correction methods in downscaling meteorological variables for a hydrologic impact study in an arid area in China, *Hydrol. Earth Syst. Sci.*, **19**, 2547–2559. https://doi.org/10.5194/hess-19-2547-2015.

Fiddes, D., Forsgate, J. A. & Grigg, A. O. (1974) *The Prediction of Storm Rainfall in East Africa*. TRRL Laboratory Report 623. Department of the Environment, Crowthorne, Berkshire.

Francisco, T. H., Menezes, O. V., Guedes, A. L., Maquera, G., Neto, D. C., Longo, O. C., Chinelli, C. K. & Soares, C. A. (2023) The main challenges for improving urban drainage systems from the perspective of Brazilian professionals, *Infrastructures*, **8**, 1–20. https://doi.org/10.3390/infrastructures8010005.

Funke, F. & Kleidorfer, M. (2024) Sensitivity of sustainable urban drainage systems to precipitation events and malfunctions, *Blue-Green Syst.*, **6**, 33–52. https://doi.org/10.2166/bgs.2024.046.

GIZ (2022) *Flooding Situation and Hotspot Analysis Report*. Technical support on the scoping for the Greater Kampala Integrated Flood Resilience Partnership.

Guptha, G. C., Swain, S., Al-Ansari, N., Taloor, A. K. & Dayal, D. (2022) Assessing the role of SuDS in resilience enhancement of urban drainage system: A case study of Gurugram City, India, *Urban Clim.*, **41**, 1–16. https://doi.org/10.1016/j.uclim.2021.101075.

Han, W. S. & Burian, S. J. (2009) Determining effective impervious area for urban hydrologic modeling, *J. Hydrol. Eng.*, **14**, 111–120. https://doi.org/10.1061/(ASCE)1084-0699(2009)14:2(111).

Havik, J. C. (2012) *The Fate and Transport of Nutrients in Shallow Groundwater and Soil of an Urban Slum Area in the City of Kampala*. Uganda: Utrecht University.

IPCC (2021) Summary for Policymakers. In: Masson-Delmotte, V., Zhai, P., Pirani, A., Connors, S. L. & Péan, C. (eds.) *Climate Change 2021: The Physical Science Basis. Contribution of Working Group I to the Sixth Assessment Report of the Intergovernmental Panel on Climate Change*, Cambridge, UK. https://doi.org/10.1017/CBO9781139177245.003.

Jiang, A. Z. & McBean, E. A. (2021) Performance of lot-level low impact development technologies under historical and climate change scenarios, *J. Hydro-Environment Res.*, **38**, 4–13. https://doi.org/https://doi.org/10.1016/j.jher.2021.07.004.

Kawai, H., Yukimoto, S., Koshiro, T., Oshima, N., Tanaka, T., Yoshimura, H. & Nagasawa, R. (2019) Significant improvement of cloud representation in the global climate model MRI-ESM2, *Geosci. Model Dev.*, **12**, 2875–2897. https://doi.org/10.5194/gmd-12-2875-2019.

Kõiv-Vainik, M., Kill, K., Espenberg, M., Uuemaa, E., Teemusk, A., Maddison, M., Palta, M. M., Török, L., Mander, Ü., Scholz, M. & Kasak, K. (2022) Urban stormwater retention capacity of nature-based solutions at different climatic conditions, *Nature-Based Solut.*, **2**, 1–13. https://doi.org/10.1016/j.nbsj.2022.100038.

Kuller, M., Reid, D. J. & Prodanovic, V. (2021) Are we planning blue-green infrastructure opportunistically or strategically? Insights from Sydney, Australia, *Blue-Green Syst.*, **3**, 267–280. https://doi.org/10.2166/bgs.2021.023.

Leandro, J. & Martins, R. (2016) A methodology for linking 2D overland flow models with the sewer network model SWMM 5.1 based on dynamic link libraries, *Water Sci. Technol.*, **73**, 3017–3026.

Leandro, J., Chen, K., Wood, R. R. & Ludwig, R. (2020) A scalable flood-resilience-index for measuring climate change adaptation: Munich city, *Water Res.*, **173**, 1–14. https://doi.org/10.1016/j.watres.2020.115502.

Lee, J., Perera, D., Glickman, T. & Taing, L. (2020) Water-related disasters and their health impacts: A global review, *Prog. Disaster Sci.*, **8**, 1–17. https://doi.org/10.1016/j.pdisas.2020.100123.

Lumbroso, D. (2018) How can policy makers in sub-Saharan Africa make early warning systems more effective? The case of Uganda, *Int. J. Disaster Risk Reduct.*, **27**, 530–540.

Maksimović, Č., Prodanović, D., Djordjević, S., Boonya-Aroonnet, S., Leitão, J. P. & Allitt, R. (2009) Overland flow and pathway analysis for modelling of urban pluvial flooding, *Hydraul. Res.*, **47**, 512–523. https://doi.org/10.3826/jhr.2009.3361.

Manchikatla, S. K. & Umamahesh, N. V. (2022) Simulation of flood hazard, prioritization of critical sub-catchments and resilience study in an urban setting using PCSWMM: A case study, *Water Policy*, **24**, 1247–1268. https://doi.org/10.2166/wp.2022.291.

Mcdonnell, J. & Motta, D. (2022) Changing rate of urban creep and urban expansion over time and its impact upon the hydrologic response of a catchment, *Water Sci. Technol.*, **85**, 383–397. https://doi.org/10.2166/wst.2021.629.

Meinshausen, M., Nicholls, Z. R., Lewis, J., Gidden, M. J., Vogel, E., Freund, M., Beyerle, U., Gessner, C., Nauels, A., Bauer, N., Canadell, J. G., Daniel, J. S., John, A., Krummel, P. B., Luderer, G., Meinshausen, N., Montzka, S. A., Rayner, P. J., Reimann, S., Smith, S. J., Van Den Berg, M., Velders, G. J., Vollmer, M. K. & Wang, R. H. (2020) The shared socio-economic pathway (SSP) greenhouse gas concentrations and their extensions to 2500, *Geosci. Model Dev.*, **13**, 3571–3605. https://doi.org/10.5194/gmd-13-3571-2020.

Mugume, S. N. (2015) *Modelling and Resilience-Based Evaluation of Urban Drainage and Flood Management Systems for Future Cities*. University of Exeter.

Mugume, S. N. & Butler, D. (2017) Evaluation of functional resilience in urban drainage and flood management systems using a global analysis approach, *Urban Water J.*, **14**, 727–736. https://doi.org/http://dx.doi.org/10.1080/1573062X.2016.1253754.

Mugume, S. N., Gomez, D. E., Fu, G., Farmani, R. & Butler, D. (2015) A global analysis approach for investigating structural resilience in urban drainage systems, *Water Res.*, **81**, 15–26. https://doi.org/10.1016/j.watres.2015.05.030.

Mugume, S. N., Gomez, D., Melville-Shreeve, P. & Butler, D. (2017) Multifunctional urban flood resilience enhancement strategies, *Proc. Inst. Civ. Eng. - Water Manag.*, **170**, 115–127. https://doi.org/10.1680/jwama.15.00078.

Mugume, S. N., Kibibi, H., Sorensen, J. & Butler, D. (2024) Can Blue-Green infrastructure enhance resilience in urban drainage systems during failure conditions?, *Water Sci. Technol.*, **89**, 915–944. https://doi.org/10.2166/wst.2024.032.

Nadoya, H. N., Ayugi, B., Onyutha, C., Babaousmail, H., Sian, K., Iyakaremye, V., Mumo, R. & Ongoma, V. (2022) Projected changes in rainfall over Uganda based on CMIP6 models, *Theor. Appl. Climatol.*, **149**, 1117–1134. https://doi.org/10.21203/rs.3.rs-894721/v1.

Nakkazi, M. T., Sempewo, J. I., Tumutungire, M. D. & Byakatonda, J. (2022) Performance evaluation of CFSR, MERRA-2 and TRMM3B42 data sets in simulating river discharge of data-scarce tropical catchments: A case study of Manafwa, Uganda, *J. Water Clim. Chang.*, **13**, 522–541. https://doi.org/10.2166/wcc.2021.174.

Neumann, J., Scheid, C. & Dittmer, U. (2024) Potential of decentral nature-Based solutions for mitigation of pluvial floods in urban areas – A simulation study based on 1D/2D coupled modeling, *Water*, **16**, 1–21. https://doi.org/10.3390/w16060811.

Ngoma, H., Wen, W., Ojara, M. & Ayugi, B. (2021) Assessing current and future spatiotemporal precipitation variability and trends over Uganda, East Africa, based on CHIRPS and regional climate model datasets, *Meteorol. Atmos. Phys.*, **133**, 823–843. https://doi.org/10.1007/s00703-021-00784-3.

O'Neill, B. C., Tebaldi, C., Van Vuuren, D. P., Eyring, V., Friedlingstein, P., Hurtt, G., Knutti, R., Kriegler, E., Lamarque, J. F., Lowe, J., Meehl, G. A., Moss, R., Riahi, K. & Sanderson, B. M. (2016) The Scenario Model Intercomparison Project (ScenarioMIP) for CMIP6, *Geosci. Model Dev.*, **9**, 3461–3482. https://doi.org/10.5194/gmd-9-3461-2016.

Ortega Sandoval, A. D., Sörensen, J., Rodríguez, J. P. & Bharati, L. (2023) Hydrologic–hydraulic assessment of SUDS control capacity using different modeling approaches: A case study in Bogotá, Colombia, *Water Sci. Technol.*, **87**, 3124–3145. https://doi.org/10.2166/wst.2023.173.

Osheen, Kansal, M. L. & Bisht, D. S. (2024) Enhancing urban drainage infrastructure through implementation of Low impact development techniques, *Water Resour. Manag*, **38**, 4517–4540. https://doi.org/10.1007/s11269-024-03877-x.

Panos, C. L., Wolfand, J. M. & Hogue, T. S. (2021) Assessing resilience of a dual drainage urban system to redevelopment and climate change, *J. Hydrol.*, **596**, 1–11. https://doi.org/10.1016/j.jhydrol.2021.126101.

Pauleit, S., Vasquéz, A., Maruthaveeran, S., Liu, L., Cilliers, S. S., (2021) Urban Green Infrastructure in the Global South. In: Shackleton, C., Cilliers, S. S., Davoren, E. & du Toit, M. (eds.) *Urban Ecology in the Global South, Cities and Nature*, Cham: Springer, pp. 107–143. https://doi.org/https://doi.org/10.1007/978-3-030-67650-6_5.

Pleau, M., Tao, D. Q., Grondin, F., Shishegar, S. & Fradet, O. (2022) Sensor fault detection for urban drainage systems using redundant measurements, *Urban Water J.*, **19**, 1038–1046.

Pons, V., Benestad, R., Sivertsen, E., Muthanna, T. M. & Bertrand-Krajewski, J. L. (2022) Forecasting green roof detention performance by temporal downscaling of precipitation time-series projections, *Hydrol. Earth Syst. Sci.*, **26**, 2855–2874. https://doi.org/10.5194/hess-26-2855-2022.

Reinstaller, S., Krebs, G., Pichler, M. & Muschalla, D. (2022) Identification of high-Impact uncertainty sources for urban flood models in hillside peri-urban catchments, *Water*, **14**, 1–25. https://doi.org/10.3390/w14121973.

Rentschler, J., Salhab, M. & Jafino, B. A. (2022) Flood exposure and poverty in 188 countries, *Nat. Commun.*, **13**, 1–11. https://doi.org/10.1038/s41467-022-30727-4.

Rhymee, H., Shams, S., Ratnayake, U. & Rahman, E. K. A. (2022) Comparing statistical downscaling and arithmetic mean in simulating CMIP6 multi-Model ensemble over Brunei, *Hydrology*, **9**, 1–15. https://doi.org/10.3390/HYDROLOGY9090161/S1.

Riahi, K., van Vuuren, D. P., Kriegler, E., Edmonds, J., O'Neill, B. C., Fujimori, S., Bauer, N., Calvin, K., Dellink, R., Fricko, O., Lutz, W., Popp, A., Cuaresma, J. C., S, K. C., Leimbach, M., Jiang, L., Kram, T., Rao, S., Emmerling, J., Ebi, K., Hasegawa, T., Havlik, P., Humpenöder, F., Da Silva, L. A., Smith, S., Stehfest, E., Bosetti, V., Eom, J., Gernaat, D., Masui, T., Rogelj, J., Strefler, J., Drouet, L., Krey, V., Luderer, G., Harmsen, M., Takahashi, K., Baumstark, L., Doelman, J. C., Kainuma, M., Klimont, Z., Marangoni, G., Lotze-Campen, H., Obersteiner, M., Tabeau, A. & Tavoni, M. (2017) The shared socioeconomic pathways and their energy, land use, and greenhouse gas emissions implications: An overview, *Glob. Environ. Chang.*, **42**, 153–168. https://doi.org/10.1016/j.gloenvcha.2016.05.009.

Ritter, A. & Muñoz-Carpena, R. (2013) Performance evaluation of hydrological models: Statistical significance for reducing subjectivity in goodness-of-fit assessments, *J. Hydrol.*, **480**, 33–45. https://doi.org/https://doi.org/10.1016/j.jhydrol.2012.12.004.

Rodriguez, M., Fu, G., Butler, D., Yuan, Z. & Cook, L. (2023) Global resilience analysis of combined sewer systems under continuous hydrologic simulation, *J. Environ. Manage.*, **344**, 1–11. https://doi.org/10.1016/j.jenvman.2023.118607.

Rosin, T. R., Kapelan, Z., Keedwell, E. & Romanoc, M. (2022) Near real-time detection of blockages in the proximity of combined sewer over fl ows using evolutionary ANNs and statistical process control, *Hydroinformatics*, **24**, 259–273. https://doi.org/10.2166/hydro.2022.036.

Rossman, L. A. (2016) *Storm Water Management Model Reference Manual Volume I – Hydrology (Revised)*. Report No. EPA/600/R-15/162A. Cincinnati, Ohio.

Ryu, J. (2008) *Decision Support for Sewer Flood Risk Management*. London: Imperial College.

Schardong, A., Simonovic, S. P., Gaur, A. & Sandink, D. (2020) Web-based tool for the development of intensity duration frequency curves under changing climate at gauged and ungauged locations, *Water (Switzerland)*, **12**, 1–31. https://doi.org/10.3390/W12051243.

Schmidli, J., Frei, C. & Vidale, P. L. (2006) Downscaling from GCM precipitation: A benchmark for dynamical and statistical downscaling methods, *Int. J. Climatol.*, **26**, 679–689. https://doi.org/10.1002/joc.1287.

Schmitt, T. G., Thomas, M. & Ettrich, N. (2005) Assessment of urban flooding by dual drainage simulation model RisUrSim, *Water Sci. Technol.*, **52**, 257–264.

Seland, Ø., Bentsen, M., Olivié, D., Toniazzo, T., Gjermundsen, A., Graff, L. S., Debernard, J. B., Gupta, A. K., He, Y. C., Kirkeväg, A., Schwinger, J., Tjiputra, J., Schanke Aas, K., Bethke, I., Fan, Y., Griesfeller, J., Grini, A., Guo, C., Ilicak, M., Karset, I. H. H., Landgren, O., Liakka, J., Moseid, K. O., Nummelin, A., Spensberger, C., Tang, H., Zhang, Z., Heinze, C.,

Iversen, T. & Schulz, M. (2020) Overview of the Norwegian Earth System Model (NorESM2) and key climate response of CMIP6 DECK, historical, and scenario simulations, *Geosci. Model Dev.*, **13**, 6165–6200. https://doi.org/10.5194/gmd-13-6165-2020.

Shrestha, M. (2016) Local intensity scaling (LOCI) bias correction. https://doi.org/10.13140/RG.2.1.5122.1367.

Siabi, E. K., Awafo, E. A., Kabo-bah, A. T., Derkyi, N. S. A., Akpoti, K., Mortey, E. M. & Yazdanie, M. (2023) Assessment of shared socioeconomic pathway (SSP) climate scenarios and its impacts on the greater Accra region, *Urban Clim.*, **49**, 1–15. https://doi.org/10.1016/J.UCLIM.2023.101432.

Sitzenfrei, R., Diao, K. & Butler, D. (2022) Resilience of interdependent urban water systems, *Water*, **14**, 1–6. https://doi.org/10.3390/w14030440.

Teutschbein, C. & Seibert, J. (2012) Bias correction of regional climate model simulations for hydrological climate-change impact studies: Review and evaluation of different methods, *J. Hydrol.*, **456–457**, 12–29. https://doi.org/10.1016/j.jhydrol.2012.05.052.

The World Bank (2022) *Living on the Water's Edge. Flood Risk and Resilience of Coastal Cities in Sub-Saharan Africa*. Washington DC, USA.

Tscheikner-Gratl, F., Caradot, N., Cherqui, F., Leitão, J. P., Ahmadi, M., Langeveld, J. G., Le Gat, Y., Scholten, L., Roghani, B., Rodríguez, J. P., Lepot, M., Stegeman, B., Heinrichsen, A., Kropp, I., Kerres, K., Almeida, M. d. C., Bach, P. M., Moy de Vitry, M., Sá Marques, A., Simões, N. E., Rouault, P., Hernandez, N., Torres, A., Werey, C., Rulleau, B. & Clemens, F. (2019) Sewer asset management–state of the art and research needs, *Urban Water J.*, **16**, 662–675. https://doi.org/10.1080/1573062X.2020.1713382.

UBOS (2020) *The National Population and Housing Census 2014–Main Report, Kampala Uganda*. Uganda Bureau of Statistics.

van Vuuren, D. P., Edmonds, J., Kainuma, M., Riahi, K., Thomson, A., Hibbard, K., Hurtt, G. C., Kram, T., Krey, V., Lamarque, J. F., Masui, T., Meinshausen, M., Nakicenovic, N., Smith, S. J. & Rose, S. K. (2011) The representative concentration pathways: An overview, *Clim. Change*, **109**, 5–31. https://doi.org/10.1007/s10584-011-0148-z.

Varlas, G., Anagnostou, M. N., Spyrou, C., Papadopoulos, A., Kalogiros, J., Mentzafou, A., Michaelides, S., Baltas, E., Karymbalis, E. & Katsafados, P. (2019) A multi-platform hydrometeorological analysis of the flash flood event of 15 November 2017 in Attica, Greece, *Remote Sens.*, **11**, 1–31. https://doi.org/10.3390/rs11010045.

Vollaers, V., Nieuwenhuis, E., van de Ven, F. & Langeveld, J. (2021) Root causes of failures in sustainable urban drainage systems (SUDS): An exploratory study in 11 municipalities in the Netherlands, *Blue-Green Syst.*, **3**, 31–48. https://doi.org/10.2166/bgs.2021.002.

Wang, M., Liu, M., Zhang, D., Zhang, Y., Su, J. & Zhou, S. (2023) Assessing hydrological performance for optimized integrated grey-green infrastructure in response to climate change based on shared socio-economic pathways, *Sustain. Cities Soc.*, **91**, 1–14. https://doi.org/10.1016/j.scs.2023.104436.

Watkins, L. H. & Fiddes, D. (1984) *Highway and Urban Hydrology in the Tropics*. Devon, England: Pentech Press Limited, Plymouth.

Webber, J. L., Fletcher, T. D., Cunningham, L., Fu, G., Butler, D. & Burns, M. J. (2020) Is green infrastructure a viable strategy for managing urban surface water flooding?, *Urban Water J.*, **17**, 598–608. https://doi.org/10.1080/1573062X.2019.1700286.

World Bank (2021) *Concept Stage Program Information Document (PID)–Greater Kampala Metropolitan Area Urban Development Program – P175660*. Washington.

Wu, T., Yu, R., Lu, Y., Jie, W., Fang, Y., Zhang, J., Zhang, L., Xin, X., Li, L., Wang, Z., Liu, Y., Zhang, F., Wu, F., Chu, M., Li, J., Li, W., Zhang, Y., Shi, X., Zhou, W., Yao, J., Liu, X., Zhao, H., Yan, J., Wei, M., Xue, W., Huang, A., Zhang, Y., Zhang, Y., Shu, Q. & Hu, A. (2021) BCC-CSM2-HR: A high-resolution version of the Beijing climate center climate system model, *Geosci. Model Dev.*, **14**, 2977–3006. https://doi.org/10.5194/gmd-14-2977-2021.

Wüthrich, D., Korswagen, P. A., Selvam, H., Oetjen, J., Bricker, J. & Schüttrumpf, H. (2024) Field survey assessment of flood loads and related building damage from the July 2021 event in the Ahr Valley (Germany), *J. Flood Risk Manage.*, 1–23. https://doi.org/10.1111/jfr3.13024.

Yang, W., Zhang, J. & Krebs, P. (2022) Low impact development practices mitigate urban flooding and non-point pollution under climate change, *J. Clean. Prod.*, **347**, 1–15. https://doi.org/10.1016/j.jclepro.2022.131320.

Yao, Y., Li, J., Jiang, Y. & Huang, G. (2023) Evaluating the response and adaptation of urban stormwater systems to changed rainfall with the CMIP6 projections, *J. Environ. Manage.*, **347**, 1–10. https://doi.org/10.1016/j.jenvman.2023.119135.

Yazdi, J. (2018) Rehabilitation of urban drainage systems using a resilience-Based approach, *Water Resour. Manage.*, **32**, 721–734. https://doi.org/10.1007/s11269-017-1835-y.

Zebaze, S., Jain, S., Salunke, P., Shafiq, S. & Mishra, S. K. (2019) Assessment of CMIP5 multimodel mean for the historical climate of Africa, *Atmos. Sci. Lett.*, **20**, 1–12. https://doi.org/10.1002/asl.926.

Zhang, X., Liu, W., Feng, Q. & Zeng, J. (2024) Multi-objective optimization of the spatial layout of green infrastructures with cost-effectiveness analysis under climate change scenarios, *Sci. Total Environ.*, **948**, 1–11. https://doi.org/10.1016/j.scitotenv.2024.174851.

First received 12 July 2024; accepted in revised form 12 September 2024. Available online 24 September 2024